Uroplakins play conserved roles in egg fertilization and acquired additional urothelial functions during mammalian divergence

Yi Liao[a,*], Hung-Chi Chang[b,c], Feng-Xia Liang[a], Pei-Jung Chung[d], Yuan Wei[a], Tuan-Phi Nguyen[a], Ge Zhou[e], Sheeva Talebian[b], Lewis C. Krey[b], Fang-Ming Deng[f,g], Tak-Wah Wong[h], Javier U. Chicote[i], James A. Grifo[b], David L. Keefe[b], Ellen Shapiro[g], Herbert Lepor[g,l], Xue-Ru Wu[f,g,j], Robert DeSalle[k], Antonio Garcia-España[i], Sang Yong Kim[f], and Tung-Tien Sun[a,g,l,m,*]

Departments of [a]Cell Biology, [b]Obstetrics and Gynecology, [f]Pathology, [g]Urology, and [l]Biochemistry and Molecular Pharmacology and [m]The Ronald O. Perelman Department of Dermatology, New York University School of Medicine, New York, NY 10016; [c]Department of Obstetrics and Gynecology, National Taiwan University, Taipei 10617, Taiwan; [d]Chang Gung University, Taoyuan 33302, Taiwan; [e]Regeneron, Tarrytown, NY 10591; [h]Department of Dermatology, National Cheng Kung University, Tainan 701, Taiwan; [i]Unitat De Recerca, Hospital Joan XXIII, Institut de Investigacio Sanitaria Pere Virgili (IISPV), Universitat Rovira i Virgili, Tarragona 43007, Spain; [j]Veterans Affairs New York Harbor Healthcare System, New York, NY 10010; [k]Sackler Institute of Comparative Genomics, American Museum of Natural History, New York, NY 10024

ABSTRACT **Uroplakin (UP) tetraspanins and their associated proteins are major mammalian urothelial differentiation products that form unique two-dimensional crystals of 16-nm particles ("urothelial plaques") covering the apical urothelial surface. Although uroplakins are highly expressed only in mammalian urothelium and are often referred to as being urothelium specific, they are also expressed in several mouse nonurothelial cell types in stomach, kidney, prostate, epididymis, testis/sperms, and ovary/oocytes. In oocytes, uroplakins colocalize with CD9 on cell-surface and multivesicular body-derived exosomes, and the cytoplasmic tail of UPIIIa undergoes a conserved fertilization-dependent, Fyn-mediated tyrosine phosphorylation that also occurs in *Xenopus laevis* eggs. Uroplakin knockout and antibody blocking reduce mouse eggs' fertilization rate in in vitro fertilization assays, and UPII/IIIa double-knockout mice have a smaller litter size. Phylogenetic analyses showed that uroplakin sequences underwent significant mammal-specific changes. These results suggest that, by mediating signal transduction and modulating membrane stability that do not require two-dimensional-crystal formation, uroplakins can perform conserved and more ancestral fertilization functions in mouse and frog eggs. Uroplakins acquired the ability to form two-dimensional-crystalline plaques during mammalian divergence, enabling them to perform additional functions, including umbrella cell enlargement and the formation of permeability and mechanical barriers, to protect/modify the apical surface of the modern-day mammalian urothelium.**

Monitoring Editor
Keith E. Mostov
University of California, San Francisco

Received: Aug 9, 2018
Revised: Oct 3, 2018
Accepted: Oct 4, 2018

INTRODUCTION

Urothelium is a multilayered epithelium, also known as transitional epithelium, that covers the luminal side of the lower urinary tract, including the renal pelvis, ureter, urinary bladder, and upper urethra. This epithelium is one of the most frequent sources of tumor formation and is the attachment site of the type 1–fimbriated *Escherichia coli*, which causes urinary tract infection. The terminally differentiated, superficial urothelial cell, known as the umbrella cell, is highly specialized, as it provides an exceptionally effective permeability barrier

This article was published online ahead of print in MBoC in Press (http://www.molbiolcell.org/cgi/doi/10.1091/mbc.E18-08-0496) on October 10, 2018.

*Address correspondence to: Yi Liao (Yi.Liao@nyumc.org) and Tung-Tien Sun (sunt01@nyumc.org).

Abbreviations used: CD, clusters of differentiation; CG, cortical granule; CTB, cholera toxin B-subunit; GM1, monosialotetrahexosylganglioside; GM3, monosialodihexosylganglioside; IF, immunofluorescence; ILV, intraluminal vesicle; IVF, in vitro fertilization; KO, knockout; LCA, lens culinaris agglutinin; MVB, multivesicular body; PVS, perivitelline space; TEM, tetraspanin-enriched microdomains; UP, uroplakin; WT, wild type; ZP, zona pellucida.

© 2018 Liao *et al*. This article is distributed by The American Society for Cell Biology under license from the author(s). Two months after publication it is available to the public under an Attribution–Noncommercial–Share Alike 3.0 Unported Creative Commons License (http://creativecommons.org/licenses/by-nc-sa/3.0).

"ASCB®," "The American Society for Cell Biology®," and "Molecular Biology of the Cell®" are registered trademarks of The American Society for Cell Biology.

(Negrete *et al.*, 1996). To perform this function, the tight junction-sealed and stretched umbrella cell is highly enlarged, being able to reach a diameter of 75–100 µm, and its apical surface is completely covered by rigid-looking plaques consisting of naturally formed two-dimensional crystals of 16-nm particles ("urothelial plaques"; 0.5- to 1-µm diameter) interconnected by the so-called hinge areas (Hicks, 1965; Kachar *et al.*, 1999). We showed that highly purified urothelial plaques contain four major integral membrane proteins, which we named uroplakins (*uro*thelial *plaque*s; abbreviated UP) (Wu *et al.*, 1990, 1994; Yu *et al.*, 1990). These are UPIa (28-kDa), UPIb (27-kDa), UPII (15-kDa), and UPIIIa (47-kDa; and several minor UPIII isoforms; see below), which are major mammalian urothelial differentiation products (Wu *et al.*, 2009; Sun *et al.*, 2013). UPIa and UPIb are tetraspanins, which interact specifically with single-spanned partner proteins uroplakins UPII and IIIa, respectively, to progressively form heterodimer (Ia/II and Ib/IIIa), heterotetramer (Ia/II-Ib/IIIa), and 16-nm particle (six heterotetramers) that are then hexagonally packed into two-dimensional crystalline arrays (Wu *et al.*, 1995; Liang *et al.*, 2001; Tu *et al.*, 2002; Hu *et al.*, 2005, 2008; Min *et al.*, 2006). Our knockout (KO) studies showed that uroplakins play important roles in the permeability barrier function and the enlargement of the terminally differentiated mouse urothelial umbrella cells (Hu *et al.*, 2000; Kong *et al.*, 2004).

Uroplakins have several paradoxical features. First, although uroplakins are highly expressed only in the plaque-forming mammalian urothelia and are often referred to as being urothelium specific (Wu *et al.*, 1994; Romih *et al.*, 2002; Olsburgh *et al.*, 2003; Sun *et al.*, 2013), they have been detected, as mRNAs or proteins, in the bladder, fat cells, and oocytes of *Xenopus laevis* (Sakakibara *et al.*, 2005; Garcia-Espana *et al.*, 2006), pronephric tubules of zebrafish (Mitra *et al.*, 2012), and several mammalian nonurothelial tissues and tumors (see *Discussion*). The significance of nonurothelial cells expressing a low amount of uroplakins is unclear. Second, Fukami, Sato, and coworkers found that in *Xenopus* eggs the tyrosine (Tyr)-phosphorylation of a UPIIIa-like protein may play an integral role in egg fertilization (Mahbub Hasan *et al.*, 2005; Sakakibara *et al.*, 2005; Sato, 2008). However, since uroplakin-II and IIIa-knockout mice are fertile (Hu *et al.*, 2000; Kong *et al.*, 2004), it is unclear whether this is a *Xenopus*-specific phenomenon. Third, our phylogenetic studies showed that uroplakin genes are highly conserved throughout vertebrate evolution including nonmammals that either have a bladder epithelium not covered by uroplakin plaques (e.g., *Xenopus laevis*) or do not even have a urinary bladder at all (e.g., fishes) (Garcia-Espana *et al.*, 2006; Garcia-Espana *et al.*, 2008; Desalle *et al.*, 2014). Taken together, these considerations raise the possibility that mammalian uroplakins may play some additional, highly conserved functions in nonurothelial cells.

Another important question has to do with the relationship among uroplakin Ia, Ib, and other tetraspanins. The tetraspanin family consists of tetra-spanned integral membrane proteins that can be divided into two groups (Garcia-Espana *et al.*, 2008; Charrin *et al.*, 2014). The first group consists of several "general" tetraspanins, including CD9, CD37, CD53, CD63, CD81, CD87, CD91, and CD151. They are widely distributed, can interact with one another to form tetraspanin-enriched microdomains, and are involved in cellular migration, interaction, fusion, infection, and fertilization (Berditchevski and Rubinstein, 2013; Termini and Gillette, 2017; van Deventer *et al.*, 2017). The second group consists of highly "specialized" and tissue-specific tetraspanins, that is, the retina-associated peripherin/RDS and Rom-1 (Goldberg *et al.*, 2016; Stuck *et al.*, 2016) and the urothelium-associated uroplakins UPIa and UPIb (Wu *et al.*, 2009; Wankel *et al.*, 2016). However, whether the tetraspanins of this second group of "specialized" tetraspanins are so sharply tissue restricted and whether they can interact with other archetypal tetraspanins of the general group is unclear.

We report here that uroplakins are made not only by mouse urothelium but also by several nonurothelial cell types, many but not all of urogenital origin, in the stomach, kidney, prostate, epididymis, testis/sperms, and ovary/oocytes. We show that uroplakin knockout and antibody blocking diminish mouse eggs' fertilization function in in vitro *fertilization* assays; that UPII/IIIa double-knockout mice have a smaller litter size; and that on fertilization the cytoplasmic tail of mouse uroplakin IIIa undergoes a conserved Fyn-mediated tyrosine phosphorylation that plays an integral role in *Xenopus laevis* egg fertilization (Mahbub Hasan *et al.*, 2005; Sakakibara *et al.*, 2005). Together with our phylogenetic data, these results indicate that uroplakins, which were first described and have been studied predominantly in mammalian urothelium, can actually perform conserved and more ancestral functions in egg fertilization and that they acquired only later during mammalian divergence their ability to form two-dimensional crystals of 16-nm particles (urothelial plaques) to perform additional functions, including umbrella cell expansion and the formation of a highly efficient permeability and mechanical barrier, –to protect and functionally modify the apical surface of the modern-day mammalian urinary bladder epithelium. Our results also indicate that the "specialized" uroplakin tetraspanins can colocalize and may interact with "general" tetraspanins such as CD9, thus blurring the artificial boundary between these two classes of tetraspanins.

RESULTS

Uroplakins can be detected in nonurothelial lineages

Existing data showed that uroplakins are highly expressed in the mammalian urothelium that covers the entire lower urinary tract, including the bladder, ureter, and renal pelvis (for a discussion of urothelium nomenclature, see Liang *et al.* [2005]). Relatively little is known about whether uroplakins are expressed in nonurothelial tissues, because some of the existing antibodies to uroplakins, although sufficiently specific for the detection of uroplakins in urothelial cells, have a relatively low signal–background ratio in nonurothelial cells (unpublished data). We improved the sensitivity and specificity of uroplakin detection in this study by using affinity-purified rabbit polyclonal antibodies against synthetic peptides or recombinant uroplakin domains, plus several newly generated mouse monoclonal antibodies listed in Table 1 (for a complete list of antibodies to uroplakins, see Supplemental Table S1). When these antibodies were used to immunoblot the proteins of purified plaques or the total urothelial extracts, they recognized its correct antigen as a single band, thus establishing their monospecificity. All the experiments were performed using multiple antibodies, with similar results. Under these conditions, we can unambiguously detect uroplakins not only in mouse urothelial upper cells (Figure 1, A1–A5, showing the detection of UPIa, II, Ib, IIIa, and IIIb) but also in the keratin 8 (K8) keratin-positive principal cells of renal medullary collecting ductal epithelium (Figure 1B), some of the K8-positive secretory cells of the anterior prostate epithelium (Figure 1C), the H+,K+-ATPase-positive, acid-secreting parietal cells of the gastric epithelium (Figure 1D), and the principal cells of cauda epididymal epithelium (Figure 1E), corneal epithelium (Figure 1F) (Adachi *et al.*, 2000), ovary (Figure 1, G–J; see below), and testis (Figure 1L and Figure 6 later in this article and Supplemental Figure S5; see below). In the following experiments, we will focus on an in-depth analysis of the ovary and testis uroplakins, which were confirmed by RT-PCR (Figure 1M).

Uroplakin	Antibody name	Epitope	Species reactivity
UPIa	AU-Ia-1 (4B4)	Mouse UPIa 2nd EC loop, 147-RLWDRIMIEQ-156	Ms, Hu, Bo
UPIa	AU-Ia-2 (3B3)	Mouse UPIa 2nd EC loop, 142-GQELTRLWDR-151	Ms, Hu, Bo
UPIa	AU-Ia-3 (3O13)	Mouse UPIa 2nd EC loop, 162-SGPMDWVNYT-171	Ms, Hu, Bo
UPIb	AU-Ib-1 (3D24)	Mouse UPIb 2nd EC loop, 40-QHSLYPLLEA-49	Ms, Hu, Bo
UPIb	AU-Ib-2 (2N23)	Mouse UPIb 2nd EC loop, 206-LGVPGYYHSQ-216	Ms, Bo
UPIb	AU-Ib-3 (3D8)	Mouse UPIb 2nd EC loop, 163-NGPSDWQKYT-172	Ms, Hu, Bo
UPIb	AU-Ib-4 (2N18)	Mouse UPIb 2nd EC loop, 177-VENNDADYPW-186	Ms, Hu
UPIIIa	AU1 (AU-IIIa-1)	Bovine UPIIIa EC domain (Liang *et al.*, 2001)	Ms, Hu, Bo
UPIIIb	AU-IIIb-1 (C362)	Mouse UPIIIb, EC domain 264-CEPGLDPLPSLSP-276	Ms, Hu
UPIIIb	AU-IIIb-2 (C341)	Mouse UPIIIb, EC domain 80-SRDFQNPQTAAKIPT-94	Ms
UPIIIb	AU-IIIb-3 (C358)	Mouse UPIIIb, EC domain 174-NPIYLHQGKNPNSID-188	Ms

All these mouse monoclonal antibodies, except AU1 (Liang *et al.*, 2001), are new. Abbreviations: EC, extracellular epitope; Bo, bovine; Hu, human; Ms, mouse.

TABLE 1: Mouse monoclonal antibodies to uroplakins.

Uroplakins are surface-expressed as heterotetramers in mouse oocytes/eggs

Our results indicate that oocyte is the uroplakin-expressing cells in the ovary and that all four major uroplakins (Ia, Ib, II, IIIa) as well as UPIIIb, a minor UPIII isoform (Deng *et al.*, 2002), are associated with the cell periphery and cytoplasmic vesicles of mouse oocytes (Figure 1G, 1–5). Although immunoblotting did not work because the tremendous dilution of the oocyte uroplakins by other uroplakin-negative ovarian cellular proteins, the staining specificity was established using at least two independent antibodies as well as by PCR (Figure 1M). Importantly, staining of the UPII-knockout mouse oocytes showed not only the expected loss of UPII but also its partner UPIa (Figure 1H, 1–5) (Kong *et al.*, 2004). Moreover, consistent with our earlier data (Deng *et al.*, 2002; Hu *et al.*, 2002), the UPIIIa-null oocytes lacked UPIIIa but retained its partner UPIb that can be stabilized by UPIIIb (Figure 1J, 1–5) (Deng *et al.*, 2002). As expected, the UP-staining pattern of the UPII/UPIIIa-double-knockout oocytes was the sum of the two single knockouts (Figure 1K, 1–5). These results confirmed the specificity of the UP staining. Moreover, we found that UPIa and II, which form the UPIa/II pair, colocalized precisely in intact mouse eggs (Supplemental Figure S1A), as did UPIb and IIIa that form the UPIb/IIIa pair (Supplemental Figure S1B). Even Ia and IIIa (members from the two pairs) colocalized (Supplemental Figure S1C), suggesting the formation of the UPIa/II-Ib/IIIa heterotetramer (Hu *et al.*, 2005). A control experiment showed that even though UPIa and CD9 colocalized precisely in some areas (see below), their global distributions were distinguishable (Supplemental Figure S1D). Taken together, these results suggest that the four major uroplakins are present in mouse eggs, which are devoid of two-dimensional uroplakin crystals, as a heterotetramer complex (UPIa/II-Ib/IIIa) (Hu *et al.*, 2005). Uroplakin staining was also seen in human ovary (Supplemental Figure S2).

Like several other egg markers, including CD9, GM1 ganglioside (a lipid raft marker), and lens culinaris agglutinin (LCA, which recognizes cortical granules; Figure 2, A, B, and E), uroplakins became polarized to the microvilli-enriched membranes during egg maturation (Figure 2, C and D), and UPIIIa knockout did not affect polarization (Supplemental Figure S3). Moreover, staining of intact oocytes and eggs showed that the UPIIIa is exposed on the cell surface (Figure 2C, 1 and 2). The use of paraffin-sections showed that although in immature oocytes UPIIIa was predominantly associated with intracellular vesicles (Figure 2D1), it became mostly surface membrane associated in mature eggs (Figure 2D2), indicating major maturation-associated translocation. In addition, developmental studies show that uroplakins were first detected in oocytes of the preantral follicles, where uroplakins were present at cell peripheries as well as cytoplasmic vesicles (Supplemental Figure S4).

In mouse eggs, uroplakins are associated with multivesicular bodies that give rise to the uroplakin-, CD9-, and CD81-positive exosomes

To determine the subcellular localization of uroplakins, we costained uroplakins with markers for various oocyte organelles. Consistent with uroplakins' integral membrane nature, they partially colocalized with an endoplasmic reticulum (ER) marker (Sec23A; Figure 2F), a Golgi marker (GM130; Figure 2G), and a late endosome marker (lysosomal associated membrane protein 1 or LAMP1; Figure 2H). They did not colocalize at all with cortical granule (Figure 2K). However, they partially colocalized with two independent markers for multivesicular bodies (MVB), that is, Alix (Figure 2M; an adaptor protein involved in intraluminal vesicle formation) (Morita *et al.*, 2007) and Hsp90 (Figure 2L2 and unpublished data). Taken together, these results indicate that uroplakins are associated with, in addition to the cell surface, the cytoplasmic MVBs.

High-resolution confocal microscopy revealed that, in many areas of the egg cell surface, uroplakins colocalized extremely well with CD9 (Figure 3A) but only partially with CD81 (Figure 3B). They also partially colocalized, in the perivitelline space (PVS) and zona pellucida (ZP), on some extracellular organelles that appeared to be exosomes based on their size, location, and antigenic properties (Figure 3, C and D). The colocalization of uroplakins with CD9 and CD81 is of interest because these two CD molecules are egg exosome markers and they are known to play key roles in egg fertilization (Miyado *et al.*, 2000; Le Naour *et al.*, 2006; Rubinstein *et al.*, 2006). The fact that uroplakins colocalized partially with CD9 and CD81 in exosomes indicates that these extracellular organelles are heterogeneous with respect to their UP, CD9, and CD81 composition (Figure 3D).

These data are confirmed and extended by the immunogold EM-labeling studies, which established the association of uroplakins with plasma membrane (Figure 3E), microvilli (Figure 3F), intraluminal vesicles of MVBs (Figure 3, G and H) (Vieira *et al.*, 2014), as well as extracellular vesicles in the PVS that are 30 to 150 nm in diameter and morphologically similar to exosomes (Figure 3I) (Meldolesi, 2018). Finally, antibodies to ovastacin produced expected staining

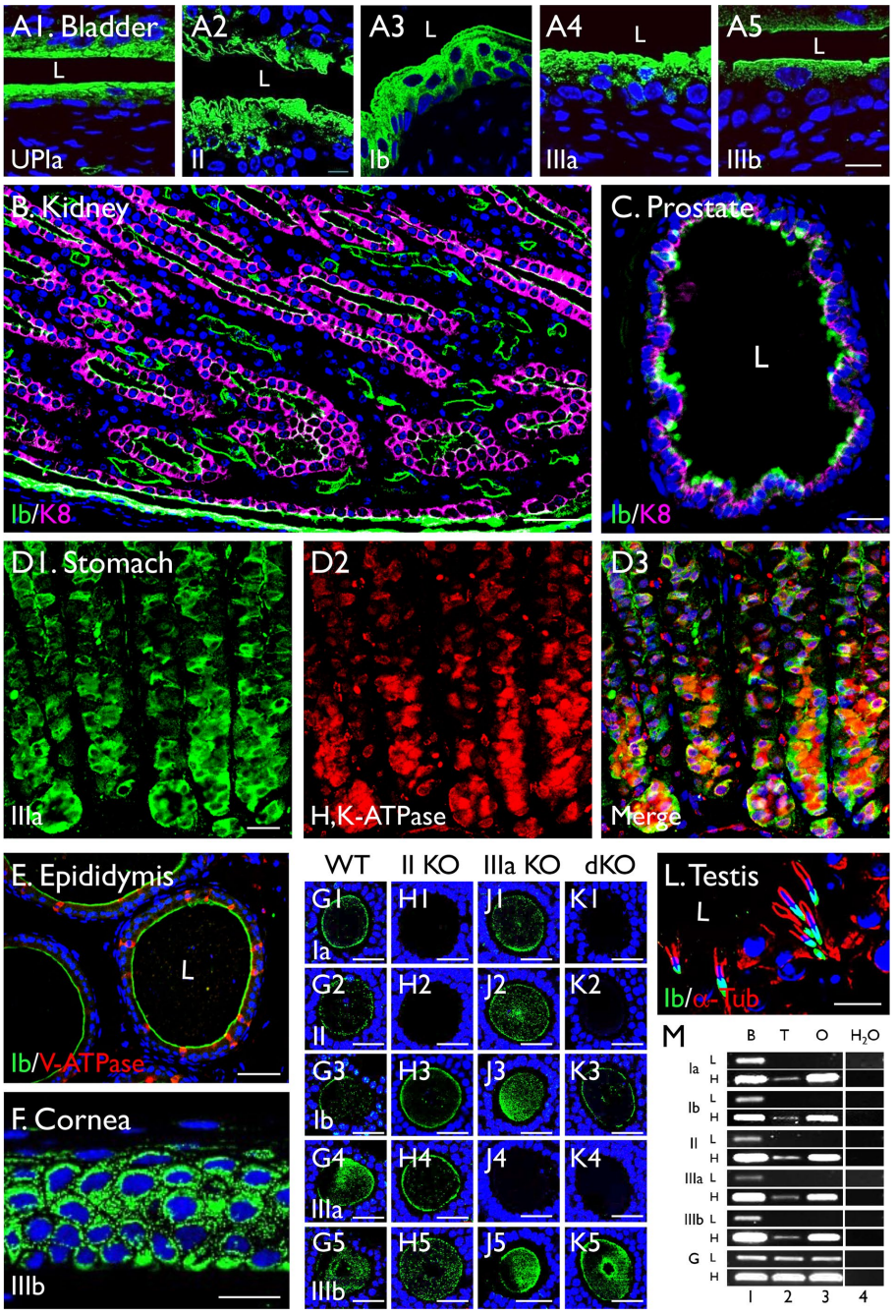

FIGURE 1: Detection of uroplakins in nonurothelial cells. Immunofluorescence staining of paraffin sections of mouse bladder urothelium (A), as well as those of nonurothelial tissues, including the (B) renal medulla, (C) anterior prostate, (D) stomach, (E) cauda epididymis, (F) cornea, (G–K) ovary, and (L) testis. Ovary samples are from (G) wild-type mouse, (H) UPII knockout, (J) UPIIIa knockout, and (K) UPII/UPIIIa double knockout. Antibodies to individual uroplakins include (A1) Ia 4867; (A2 and L) Ib 7472; (B, C, E) 7727; (A3) II 160; (A4) IIIa 182; (D) 35804; and (F) IIIb 6177; for the description of these antibodies, see Table 1 and Supplemental Table S1). Other antibodies include alpha-tubulin (α-Tub), K8, V-ATPase, and H+,K+-ATPase, as noted. (M) Detection of uroplakins mRNAs by RT-PCR in bladder (lane 1; B), testis (2; T), ovary (3; O), or water control after 30 (low, L) or 35 (high, H) cycles Glyceraldehyde 3-phosphate dehydrogenase (GAPDH) control. Note the detection of uroplakins in B the apical surface of the K8-positive renal collecting duct, (C) the upper parts of some of the K8-positive secretory prostatic epithelial cells, (D) the H+,K+-ATPase-positive gastric parietal cells, (E) the apical surface of the V-ATPase-negative epididymal epithelial cells, (F) the corneal epithelium, (G–K) oocytes, and (L) spermatids in testis. Also note in G to K the absence of UPII (and its partner UPIa) and UPIIIa in the UPII- and UPIIIa-KO oocytes, respectively, thus confirming the specificity of the uroplakin staining. L = lumen. Nuclear staining: DAPI (A–F) or To-Pro-3 (G–K). Bars equal to 10 μm (A, C, F, and L), 50 μm (B, E), 20 μm (D), or 30 μm (G–J).

of cortical granules (Figure 3J) that are morphologically distinct from the UP-positive multivesicular bodies (Figure 3, G and H) that, in UPII-knockout eggs, are replaced by abnormal multilobular structures (Figure 3K).

Mouse uroplakin IIIa undergoes conserved tyrosine-phosphorylation on egg fertilization

Of the four major uroplakins (Ia/II and Ib/IIIa), UPIIIa is the only one that has a long cytoplasmic tail that is known to play a signaling function (Thumbikat *et al.*, 2009). Fukami, Sato, and coworkers showed that in *Xenopus* eggs a UPIIIa-like protein undergoes Src-mediated Tyr-phosphorylation in a $TY^{249}SS(T/A)$ motif and that antibody to the extracellular domain of this uroplakin abolishes *Xenopus* egg fertilization (Mahbub Hasan *et al.*, 2005; Sakakibara *et al.*, 2005; Mahbub Hasan *et al.*, 2007). Since the molecular players involved in sperm–egg interaction/fertilization can vary even among mammalian species (Evans, 2012), and since a similar $(S/A)Y^{266}(S/T)SV$ motif is conserved in all mammalian UPIIIs (Supplemental Figure S6D), we wanted to see whether this fertilization-dependent event occurs in the evolutionarily distant mouse eggs.

To confirm this phosphorylation event in *Xenopus* oocytes, we made antibodies against all five frog uroplakins, that is, xUPIa, xUPIb, xUPII, xUPIIIa, and xUPIIIb, which we described earlier as cDNAs (x stands for *Xenopus*) (Garcia-Espana *et al.*, 2006); of these, only xUPIb and xUPIIIb have been studied as proteins (Mahbub Hasan *et al.*, 2005; Sakakibara *et al.*, 2005). We also made sequence-specific antibodies against the nonphosphorylated and Tyr^{249}-phosphorylated peptide of xUPIIIa (see Supplemental Table S1 for a list of antibodies to uroplakin proteins and peptides). Antibodies to all five uroplakins stained the superficial cells of *Xenopus* bladder epithelium (unpublished data), as well as the cell surface of *Xenopus* oocytes and mature eggs (Figure 4, A–F); none of them known to have two-dimensional crystalline plaques. Although the untreated eggs had no detectable Tyr-phosphorylation of UPIIIa and Src (Figure 4, M and N), sperm-fertilized and H_2O_2-activated *Xenopus* eggs showed the phosphorylation of Tyr^{249} of xUPIIIa (Figure 4, P and V) as well as Tyr^{416} of Src (Figure 4, Q and W). Control experiments confirmed that tyrosine phosphorylation of both xUPIIIa and Src in sperm-fertilized eggs was blocked by a rabbit antibody to the extracellular domain of xIIIa (Figure 4, S and T) (Sakakibara *et al.*, 2005), and showed that the reactions in peroxide-activated eggs

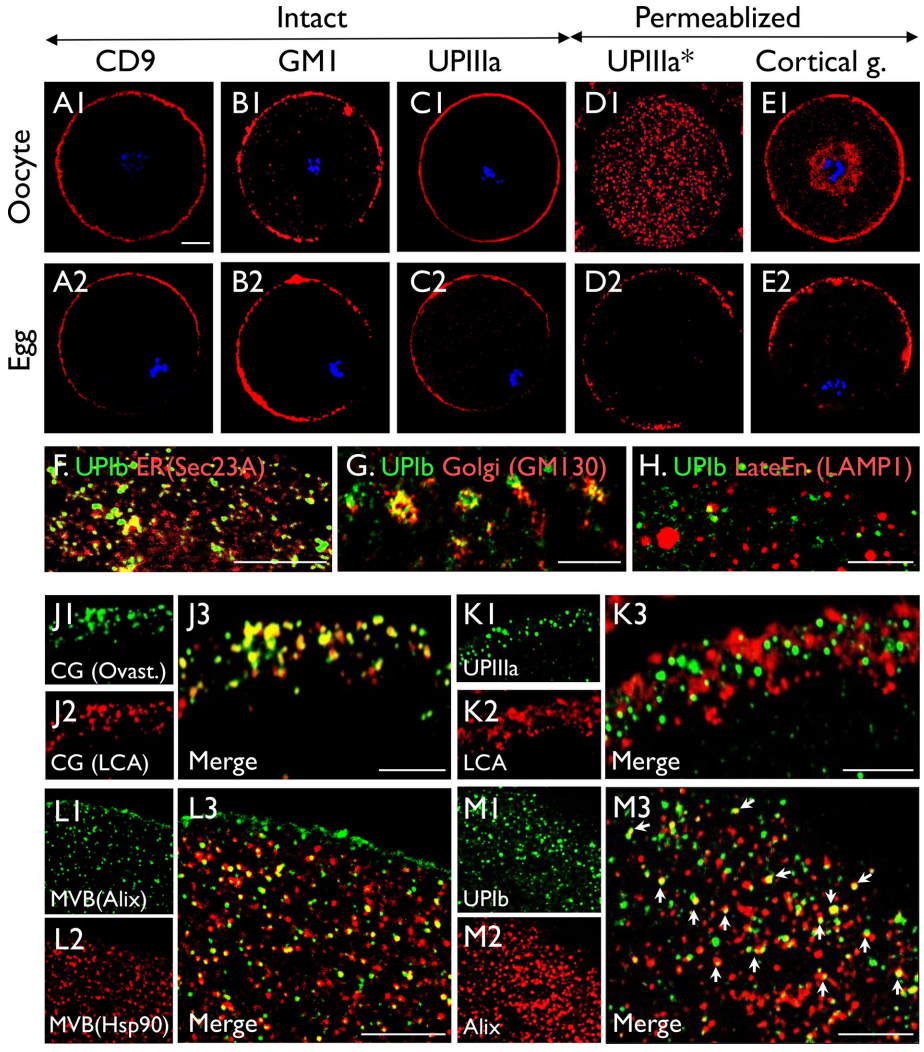

FIGURE 2: Colocalization of uroplakins with CD9 and CD81 in polarizing mouse oocytes. (A–E) immunofluorescence staining of immature oocytes (A1–E1) and mature eggs (A2–E2) using (A) anti-CD9, (B) Cholera toxin (CTB, recognizing ganglioside GM1, a raft marker); (C, D) anti-uroplakin IIIa (35804); and (E) LCA). The staining was performed using intact oocytes and eggs (A, B, C), Triton X-100–treated samples (E), or paraffin sections (D*). Note the relatively even surface-association of uroplakins and other surface markers in immature oocytes (A1–E1), and their polarization to the microvilli-rich pole on egg maturation (A2–E2). Also note the abundant cytoplasmic UP vesicles in permeabilized oocytes (D1), and their predominant polarized surface-association in mature eggs (C2, D2). (F–M) Oocytes were double-stained using antibodies to (F) UPIb (AU-Ib-2)/Sec23A (ER marker); (G) UPIb (AU-Ib-2)/GM130 (Golgi); (H) UPIb (7472)/LAMP1 (late endosome); (J) ovastacin/LCA (both cortical granule markers; note precise colocalization); (K) UPIIIa (35804)/LCA; (L) Hsp90/Alix (both multivesicular body markers); (M) UPIb (7472)/Alix. Note in M the partial colocalization of UPIb with Alix. Bars equal to 10 μm (A-E) or 5 μm (F–M).

were blocked by a Src inhibitor SKI-606 (Figure 4, Y and Z). These results showed, for the first time, that all five major x-uroplakins proteins cover the *Xenopus* oocyte surface (Figure 4, B–F) and confirmed that onfertilization Tyr^{249} of xUPIIIa undergoes Src-mediated phosphorylation (Mahbub Hasan *et al.*, 2005).

We next examined the possible phosphorylation of Tyr^{266} of mouse UPIIIa (in the same motif as Tyr^{249} of *Xenopus*). While control mouse eggs had no detectable Tyr^{266}-phosphorylation (Figure 5D), ethanol activation of mouse eggs led to Tyr^{266} phosphorylation (Figure 5E), which was blocked by Src-inhibitor SU6656 (Figure 5F). Interestingly, egg activation also led to the phosphorylation of Tyr^{418} in Fyn, the major Src-related kinase in mouse oocytes (Figure 5, J and K), and this event was also blocked by SU6656 (Figure 5L). The specificity of the phosphorylation was shown in a control, indicating that the amount of total phosphorylated tyrosine (detected by a pan anti-phosphotyrosine antibody) rose tremendously on egg activation (Figure 5, M and N), and this was also SU6656 sensitive (Figure 5O). High-resolution confocal microscopy revealed that the UPII, Fyn, and CD9 colocalized in discrete patches (Figure 5P) and that, after fertilization, the Tyr-phosphorylated UPIIIa and Fyn remained colocalized (Figure 5Q). Notably, UPIa barely colocalized with GM1, a raft marker, indicating that the uroplakin-containing tetraspanin-enriched microdomains, like that of other tetraspanins (Claas *et al.*, 2001; Le Naour *et al.*, 2006), are distinct from the conventional GM1-positive rafts (Figure 5R) (Hemler, 2003, 2005). These results indicate that uroplakin, Fyn kinase, and CD9 are concentrated in the tetraspanin-enriched microdomains and that on fertilization Fyn phosphorylates Tyr^{266} of UPIIIa as a signaling step involved in mouse egg fertilization (see *Discussion*).

Uroplakins are associated with the mouse sperm hook

Immunofluorescence staining showed that all five uroplakins are also associated with the head of spermatids in mouse testis (Figure 6, A and B, and Supplemental Figure S5) and of mature sperms (Figure 6, C–M). The specificity of these staining data was supported by the fact that the staining of UPII (and its partner UPIa) was abolished in the UPII-knockout sperms (Figure 6D) and that UPIIIa staining was abolished in the UPIIIa-knockout sperms (Figure 6E). While most of the uroplakins were associated with the sperm hook, there were small patches of perhaps less tightly bound uroplakins elsewhere in the head (Figure 6, C–E and H). Although the detection of the intracellular α-tubulin and Sp56 (an acrosome marker) required Triton-permeabilization (Figure 6, G and K2), uroplakins were readily detected on intact sperms (Figure 6, F and J1), indicating that they are surface exposed. Double staining with Sp56 showed that the uroplakins are associated primarily with the rostral hook abutting the Sp56-positive acrosome (Figure 6K4). The morphology of the UP-associated hook remains unchanged in uroplakin II- and IIIa-knockout sperms (Figure 6, D, E, L1, and M1).

Uroplakin deficiency reduces the fertilization function of mouse eggs

To assess the functional significance of uroplakins in mouse eggs and sperms, we performed in vitro fertilization assays (IVF) (Figure 7, A–C). The results indicate that while the wild-type mouse gametes have an in vitro fertilization rate of ~82%, those of the UPII KO, UPIIIa KO, and double KO dropped to 47, 41, and 39%, respectively;

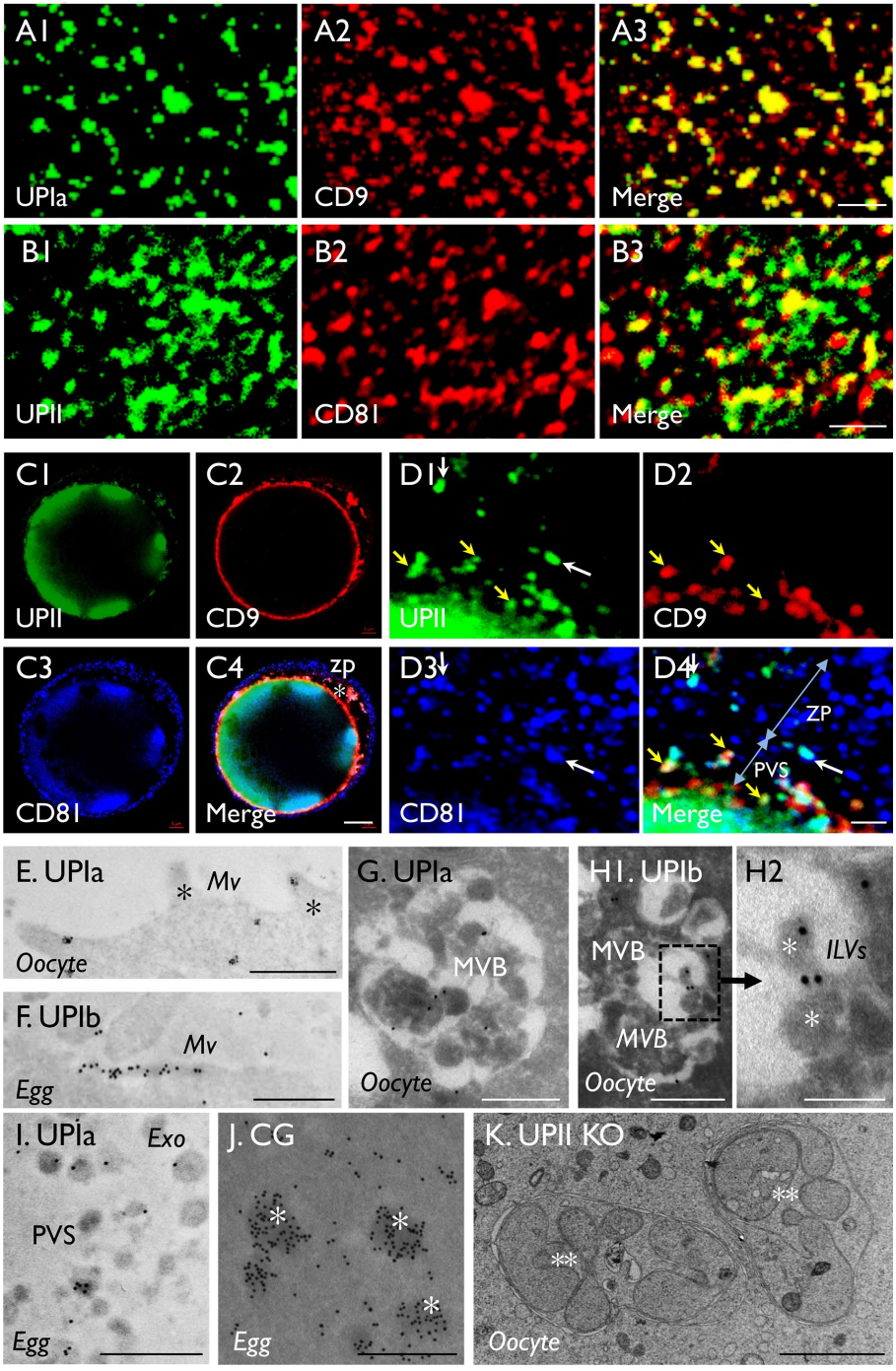

FIGURE 3: Uroplakin association with cell-surface, multivesicular bodies, and exosomes of mouse oocytes. (A, B) Colocalization of uroplakins with (A) CD9 and (B) CD81 at egg plasma membranes (zona pellucida free). (C, D) Colocalization of UPII (S3045), CD9, CD81 by IF-staining of intact eggs with intact zona pellucida viewed at (C) low or (D) high magnification. Note that in A and B the precise and partial colocalization of UP with CD9 and CD81, respectively; in D the partial colocalization of UPII and CD9 on the exosomes in the PVS (yellow arrows) and the colocalization of UPII and CD81 on some exosomes in ZP (white arrows). Blue nuclear staining by Hoechst 33258 in C and D. (E–J) IEM localization by staining ultrathin sections of oocytes (E, G, H) or eggs (F, I, J) using antibodies to UPIa (E, G, I) and Ib (F, H) and ovastacin of cortical granules (J). Note the association of UP's with oocyte surface (E), egg microvilli (F), multivesicular bodies (G, H1) and their intraluminal vesicles (H2; asterisks), and exosomes (I). Note the distinct staining patterns of the uroplakin-positive MVBs (G, H1) and cortical granules (J; asterisks). (K) Transmission electron microscopy of an egg from a UPII-knockout mouse showing unusual multilobular bodies (**) possibly representing autophagasomes. Uroplakin antibodies: (A, E, and I, Ia128; B, C, and D, II S3045; and F and H, Ib 7727). Bars equal to 2 μm (A, B, D, and K), 10 μm (C), 0.5 μm (E-G, H1, I and J), or 0.2 μm (H2).

in all these cases the blastocyst formation rates were not significantly affected (Figure 7A). To assess the effects of UP deficiency on male vs. female gametes, we repeated the IVF assays using gametes from normal mice in combination with gametes from the UP-null mice of the opposite sex. The results showed that eggs from the UPII KO and UPIIIa KO mice had reduced fertilization rates of 42 and 34%, respectively, indicating that uroplakins play an essential role in egg fertilization (Figure 7B). However, sperms from the UPII KO, UPIIIa KO, and double-KO mice had normal fertilization rates of 87, 89, and 77%, respectively, indicating that uroplakin-null sperms function normally in the setting of this in vitro assay (Figure 7C; see *Discussion*). The importance of uroplakins in egg fertilization was supported by the fact that preincubation of normal eggs with antibodies against the extracellular epitopes of CD9, UPIa, and UPIb reduced the in vitro fertilization from 68% to 40, 32, and 7%, respectively (Figure 7D). Although an antibody to UPIIIa failed to block fertilization, it is possible that this was due to the inaccessibility of its particular epitope. Finally, we assessed the litter size of the UPII-, UPIIIa- and double-knockout mice. Although the litter sizes of the UPII KO and UPIIIa KO mice were in the normal range (Hu *et al.*, 2000; Kong *et al.*, 2004), those of the double-KO mice were significantly reduced from an average of 11–6 (Figure 7E).

Emergence of mammal-specific uroplakin sequences

On the basis of the *fully sequenced genomes* of a broad array of chordates (cephalochordats, urochordates, and vertebrates), we have previously analyzed the evolution of uroplakin genes and showed that they originate in the common ancestor of vertebrates (Garcia-Espana *et al.*, 2006; Desalle *et al.*, 2014; Chicote *et al.*, 2017). Analyses of the vertebrate uroplakin sequences revealed many mammal-specific residues interspersed by residues that are common to all (mammalian and nonmammalian) uroplakins (Figure 8, A and B, and Supplemental Figure S6) (Desalle *et al.*, 2014). It is likely that the amino acid residues that are common to all vertebrates are involved in forming the basic tetraspanin structure and playing ancestral functions in nonurothelial cells, including egg fertilization, whereas some of the mammal-specific residues may contribute to two-dimensional crystal formation and other mammal-specific functions (Figure 8, A and B, and Supplemental Figure S6). Finally, of all the uroplakins, UPIb stood out as having the smallest number of

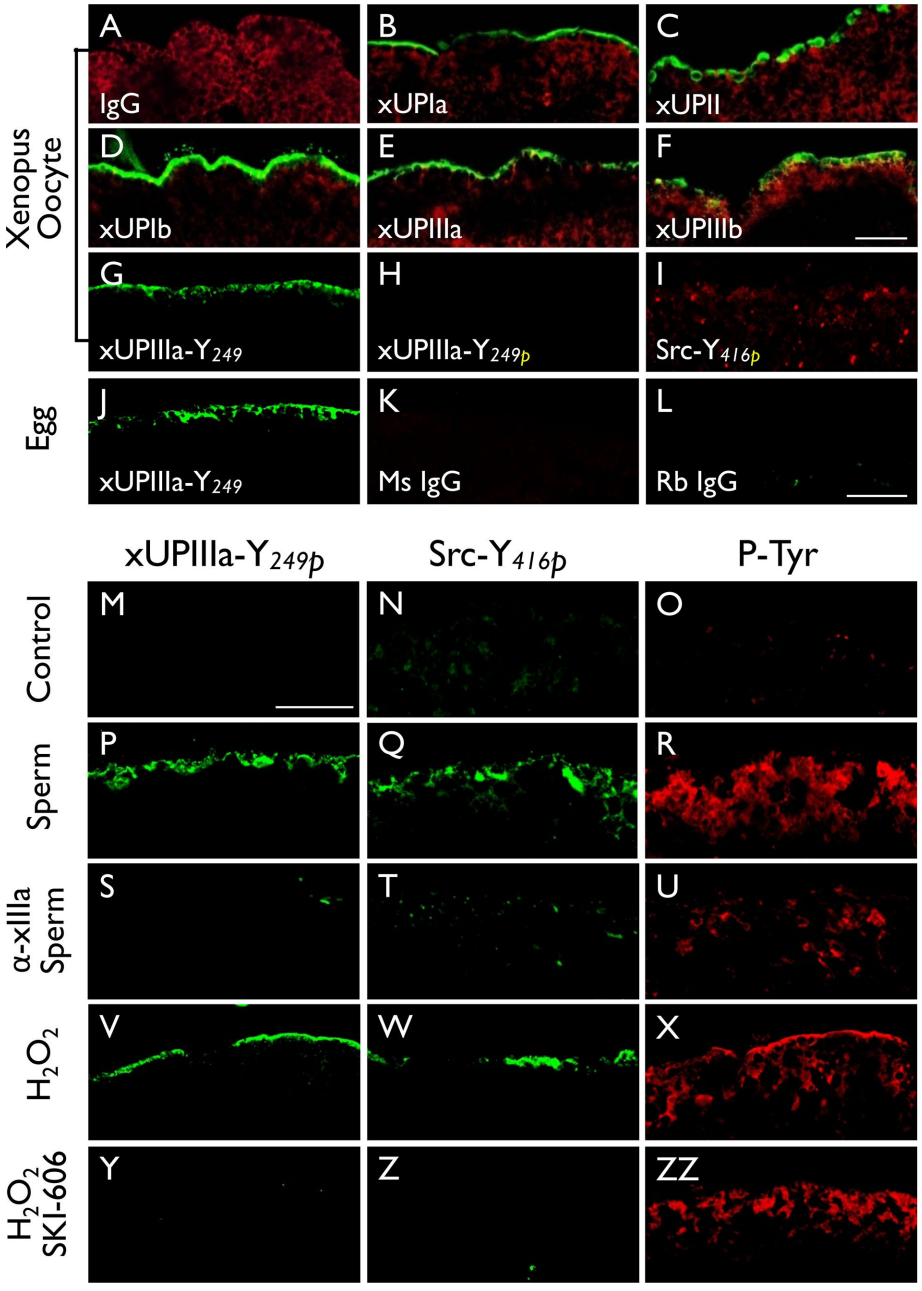

FIGURE 4: Fertilization of *Xenopus* laevis (Xl) eggs led to tyrosine phosphorylation of UPIIIa and Src. *Xenopus* oocytes (A–I) were stained using (A) normal IgG (negative control), or antibodies to (B) *Xenopus* UPIa or xUPIa (19228), (C) xUPII (13641), (D) xUPIb (13638), (E) xIIIa (19230), (F) xIIIb (4865), (G) xIIIa-Y249 (nonphosphorylated peptide, 35761), (H) xIIIa-Y249P (Tyr-phosphorylated peptide, 35760), or (I) Src-Y416 (Tyr-phosphorylated peptide). Alpha-tubulin was colocalized in A–F as a control. Note the detection of all five *Xenopus* homologues of mammalian uroplakins on the egg surface. (J–L) *Xenopus* eggs were stained using antibodies to (J) xIIIa-Y249, (K) normal mouse IgG, or (L) normal rabbit IgG. (M–ZZ) immunofluorescence staining was done using (M–O) control *Xenopus* eggs, (P–R) sperm-fertilized eggs, (S–U) eggs pretreated with an antibody to xUPIIIa before sperm fertilization, (V–X) hydrogen peroxide-activated eggs, and (Y–ZZ) SKI-606–pretreated eggs before hydrogen peroxide activation. In this series of experiments, each type of egg was stained using antibodies to xIIIa Y249P (first column), Src-Y416P (second), and pan phosphorylated-tyrosine (third). Note the increased Y-phosphorylation of xIIIa and Src in both sperm-fertilized (P, Q) and peroxide-activated (V, W) eggs and the blockage of this reaction by an anti-xUPIIIa antibody (S, T) and Src inhibitor SKI-606 (Y, Z). Bars equal to 20 μm.

mammal-specific sequences (13%; vs. 55% common sequence), compared with all other uroplakins: UPIa (33%, 40%), UPII (49%; 21%), UPIIIa (36%; 27%), and UPIIIb (27%; 25%) (Figure 8B).

DISCUSSION

Uroplakins of the nonurothelial cells

In this first systematic study of uroplakins in nonurothelial cells, we found that uroplakins are present (roughly 5–10× lower level than urothelium) in several mouse nonurothelial cells, many but not all of them are of urogenital origin. These include the K8-positive renal collecting ducts (Figure 1B). Even though we and others have described uroplakin mRNAs and/or proteins in kidney samples, these earlier results can be accounted for by the presence of urothelium in renal pelvis (Adachi *et al.*, 2000; Sakakibara *et al.*, 2005; Garcia-Espana *et al.*, 2006; Carpenter *et al.*, 2016). The expression of uroplakins in renal collecting ducts (Figure 1B) offers a more direct explanation for how UPIIIa mutations may cause renal adysplasia that can lead to severe kidney failure (Jenkins *et al.*, 2005) and suggests that some of the uroplakin-containing urine exosomes may be derived from the kidney, instead of the umbrella cell (Pisitkun *et al.*, 2004), which is not known to make a significant amount of exosomes (Figure 9B). In addition, we found uroplakin accumulation in the 1) upper part of some of the K8-positive secretory cells of the anterior prostate (Figure 1C); 2) H^+,K^+-ATPase-positive, acid-secreting parietal cells of the stomach (Figure 1D); 3) apical surface of the cauda epididymis (but not the V-ATPase-positive narrow cells; Figure 1E); 4) corneal epithelium, which expresses UPIb/IIIb (Figure 1F) (Adachi *et al.*, 2000; Swamynathan *et al.*, 2008); 5) ovary (Figure 1, G–K), 6) spermatids (Figures 1L and 6 and Supplemental Figure S5); and 7) mesothelium (unpublished data) (Kanamori-Katayama *et al.*, 2011; Rudat *et al.*, 2014). Finally, a minor subpopulation of UPIIIa-positive murine lung epithelial "club cells" were recently reported to be the progenitor cells that give rise to ciliated cells (Guha *et al.*, 2017). Taken together, these results indicate that, although uroplakin provides a highly sensitive urothelial marker (Moll *et al.*, 1995; Huang *et al.*, 2007; Hoang *et al.*, 2015; Tian *et al.*, 2015), tumors derived from certain nonurothelial cells or from a minor subpopulation of uroplakin-positive cells in a mostly uroplakin-negative tissue, such as kidney (Figure 1B), prostate (Figure 1C), or stomach (Figure 1D), can be uroplakin positive. In such cases, uroplakin staining of the tumors could be of additional differential diagnostic value. Finally, although uroplakin mRNAs have been detected in some other cell types by, for example, RNAseq, these messages often remain untranslated (see, e.g., Carpenter *et al.* [2016] and Human-Protein-Atlas [2018]). Thus, for most purposes of cell/tumor identification it is in general more reliable to detect the uroplakin proteins.

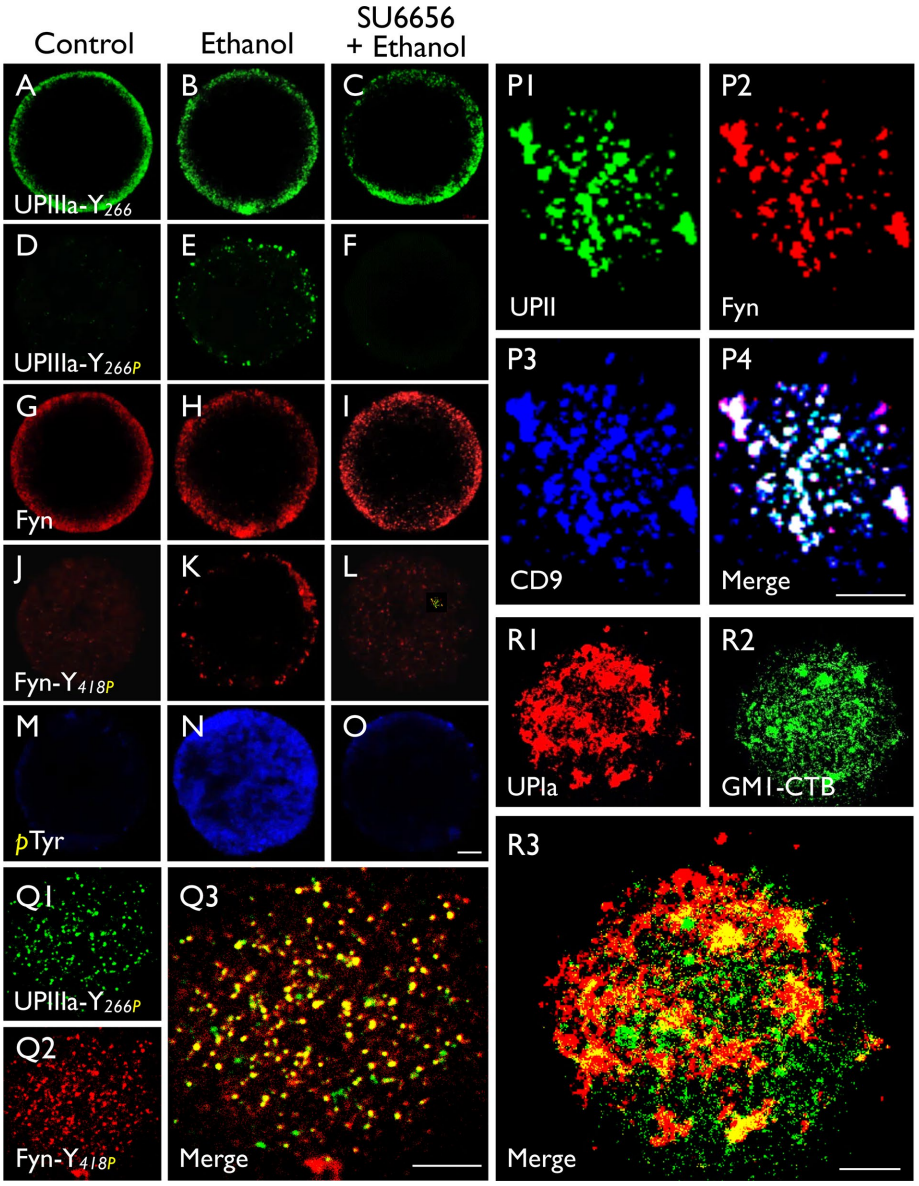

FIGURE 5: Parthenogenetic activation of mouse eggs led to the tyrosine-phosphorylation of UPIIIa and Fyn. Permeabilized normal eggs (control; first column), ethanol-activated eggs (second column), and SU6656 (Fyn inhibitor)-pretreated and ethanol-activated eggs (third column) were stained using antibodies to (A–C) UPIIIa-Y266 (35759), (D–F) UPIIIa-Y266P (35758) (synthetic peptide containing the phosphorylated (P)-Tyr 266), (G–I) Fyn, (J–L) Fyn-Y418P (synthetic peptide containing the phosphorylated Tyr 418 of Fyn, and (M–O) phosphorylated Tyr. Note in the second column that ethanol-activation led to the Tyr-phosphorylation of UPIIIa-Y266 (E) and Fyn-Y418 (K), and their blockage by SU6656 (third column). (P–R) Immunostaining of intact mouse eggs with antibodies to (P) UPII (S3045)/Fyn/CD9, (Q) UPIIIa-Y266P/Fyn-Y418P, and (R) UPIa/GM1-CTB (a raft marker). Note that in P the substantial colocalization of UPII/Fyn with CD9; in Q the colocalization of tyrosine-phosphorylated UPIIIa and tyrosine-phosphorylated Fyn; and in R the poor colocalization between UPIa (AU-Ia-1) and the raft marker GM-1. Bars equal to 10 μm (A–O) or 5 μm (P–R).

Our finding that uroplakin expression is less urothelium-restricted than previously thought raises a cautionary note about the use of uroplakin promoters to drive urothelial expression of transgenes for developing mouse models of bladder tumorigenesis and other urinary tract diseases (see, e.g., Lin *et al.*, 1995[1]; Wu, 2009; Schnegelsberg *et al.*, 2010). Although in most of these studies the transgenes targeted mainly urothelium and generated useful models, some studies showed unexpected targeting of nonurothelial tissues such as the lung (Ahmad *et al.*, 2011; Ayala de la Pena *et al.*, 2014), which may be explained by this work. In future studies, the urothelial specificity of uroplakin promoters can be further improved, if needed, by using an inducible system coupled with the intravesicle delivery of the doxycycline or tamoxifen inducer (Zhou *et al.*, 2010; Van Batavia *et al.*, 2014).

Distinct trafficking patterns of uroplakins in oocytes and urothelial umbrella cells

Our data indicate that the uroplakin trafficking patterns of the eggs and urothelial cells are distinct (see models in Figure 9). Thus, in mouse oocytes where a low level of uroplakins are targeted to the cell-surface and MVB-derived exosomes, these proteins are delivered from the ER/Golgi either via small exocytotic vesicles (Figure 2D1) to the cell surface (Figure 2D2), or to the MVBs (Figures 2M and 3, G and H), which then give rise to the UP-, CD9-, and/or CD81-positive exosomes (Figures 3, D and I, and 9A). In urothelial umbrella cells, where a huge amount of uroplakins is targeted predominantly to the apical surface, they are first assembled in post-Golgi vesicles into two-dimensional crystals of 16-nm particles (with six tetramers), which are delivered via specialized discoidal (DV) and fusiform vesicles (FV) to the apical surface (Wankel *et al.*, 2016; Gallo *et al.*, 2018) and then endocytosed for MVB/lysosome-mediated degradation (Figure 9B) (Khandelwal *et al.*, 2009; Vieira *et al.*, 2014). It should be noted, however, that even though the major uroplakin pathways (thick arrows in Figure 9) differ in these two cell types, they do overlap (Figure 9).

Possible roles of uroplakins in fertilization

An important conclusion of our work is that uroplakins, which were discovered as major mammalian urothelial differentiation products and have been studied predominantly in this epithelium (Wu *et al.*, 2009; Sun *et al.*, 2013; Wankel *et al.*, 2016), perform essential functions in mouse egg fertilization. This conclusion is based on our observations that antibodies to the extracellular domains of UPIa and Ib reduced the in vitro fertilization rate of mouse eggs (Figure 7D) and that UPII/IIIa double-knockout mice had a smaller litter size (Figure 7E). These results are consistent with earlier finding by Fukami, Sato, and coworkers, who showed that antibodies to the extracellular domain of xUPIIIa abolishes the fertilization of eggs from the distant *Xenopus* (Sakakibara *et al.*, 2005). Taken together,

[1]He F, Wu XR, Sun T-T (2017). UPII Promoter: an update, http://sun-lab.med.nyu.edu/protocols-reagents/sun-lab-reagents.

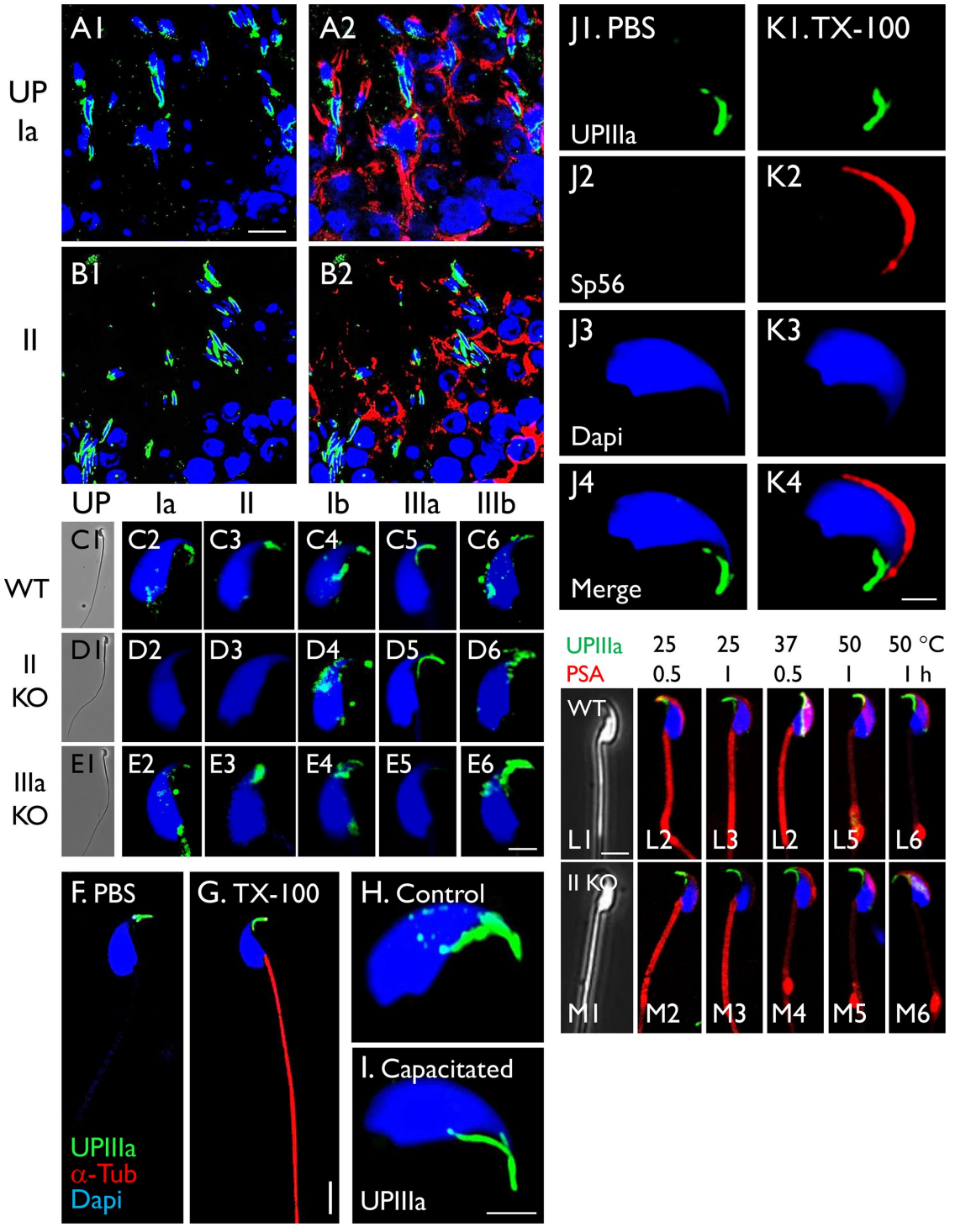

FIGURE 6: Association of uroplakins with the mouse sperm head. (A, B) Paraffin-sections of mouse testis were triple-stained using antibodies to uroplakins Ia (4867) or II (160) (green), alpha-tubulin (red) and To-Pro-3 (blue; nuclei). (C–E) Uroplakin staining of intact mouse sperms from (C) wild-type, (D) UPII-knockout, and (E) UPIIIa-knockout mouse using antibodies to specific uroplakins as noted. (F, G) Staining of mouse sperms that have been treated with (F) PBS or (G) 0.1% Triton X-100. (H, I) UPIIIa staining of a control sperm (H) or a capacitated sperm (I). (J, K) Triple staining of control sperms (J) or those pretreated with 0.1% Triton X-100 (K), using antibodies to UPIIIa, Sp56 (acrosome marker) and DAPI. (L, M) Double-staining of sperms (that have been heat-treated) using anti-UPIIIa and PSA. Antibodies to uroplakins are as follows: Ia, AU-Ia-1; II, S3045; Ib, AU-Ib-2; IIIa, 35804; IIIb, 6177 (Table 1 and Supplemental Table S1). Note in H, I, J, and K the UP-staining of the sperm heads, in D the absence of UPII and its partner Ia in the UPII-null sperms, and in E the absence of UPIIIa in the IIIa-KO sperms. Also note in L that heat treatment had little effects on hook-associated UP-staining, and led to the formation of abnormal PSA stained swelling near the transitional zone between the mid-body and tail. The sperms were collected from cauda epididymis, and nuclear staining was by DAPI. Bars equal to 10 μm (A, B), 5 μm (F, G, L, and M), or 2 μm (C–E, H–K).

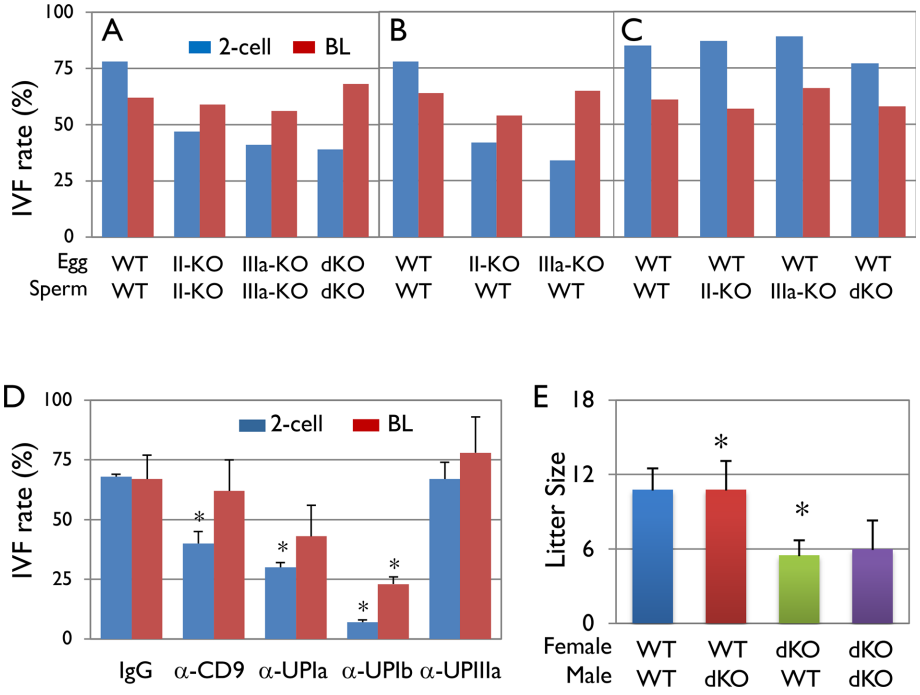

FIGURE 7: Effects of uroplakin knockout on mouse gamete fertilization. (A–C) Uroplakin-deficient eggs had a reduced fertilization rate. IVF assays using (A) uroplakin knockout eggs and sperms, (B) uroplakin knockout eggs and WT sperms, and (C) WT eggs and uroplakin knockout sperms. Note in A that uroplakin deficiency impaired the fertilization (2-Cell; blue bars) but not embryonic development (Blastocyst, BL; red bars), and in B and C that this impairment was caused by UP deficiency in eggs. Eggs and sperms were collected from 8 to 10 female and two to three male mice for each group, respectively. (D) Effects of anti-uroplakin antibodies on the in vitro fertilization of the mouse eggs; 5 WT female mice were used for each group. The antibodies used are affinity-purified rabbit antibodies to the extracellular domains of mouse UPIa (128) and UPIb (7727), and to a mouse UPIIIa synthetic peptide corresponding to a juxta-membrane epitope (position 179–191 QTLWSDPIWTNRP(C)). The ZP-intact WT eggs were preincubated with these antibodies (final concentration 200 μg/ml) for 30 min prior to incubation with WT sperms. Error bars are the SD of four independent groups. Asterisks mark values that are significantly different from the controls ($p < 0.01$, one-way analysis of variance [ANOVA]). (E) In vivo pup production: The litter sizes of various breeding combinations between the WT and double-UP-knockout mice. Note that pairs involving only female, but not male, KO mice had a reduced litter size. Five breeding pairs (8–12 wk old) were used for each group, and four to five litters were produced from each pair. Error bars are the SD of five independent groups. Asterisks denote statistical significance ($p < 0.01$, one-way ANOVA).

these data suggest that uroplakins perform important, conserved functions in egg fertilization.

Although the precise function of uroplakins in egg fertilization is unclear, their association with the plasma membrane and particularly notably the microvilli of eggs (Figures 2, A–C, and 3, E and F), as well as egg-associated exosomes (Figure 3, D, G, and H), suggests that they perform membrane-related fertilization functions, including sperm–egg interactions and the formation and/or modulation of exosomes that play a critical role in egg–sperm fusion (Harada *et al.*, 2013). Regarding the surface-related function, it has been suggested that xUPIIIa may serve as a sperm receptor, based on the observation that an antibody to its extracellular domain reduced *Xenopus* egg fertilization (Mahbub Hasan *et al.*, 2005). In this regard, it is of interest to note that in our studies antibodies to Ia and Ib, but not IIIa (possibly due to the inaccessibility of the juxta-membrane epitope), reduced mouse egg in vitro fertilization (Figure 7D). This suggests that antibody binding to uroplakins Ia and Ib may induce global structural changes of the uroplakin complex (see, e.g., Wang *et al.* [2009]), thus hampering UPIIIa signaling and egg fertilization, and that antibody blocking data per se do not necessarily mean that the protein antigen(s) is a sperm receptor. Overall, existing data suggest that uroplakins participate in the following cellular processes in fertilization.

Signal transduction

Egg fertilization triggers Tyr phosphorylation of UPIIIa. Of the four major uroplakins, UPIIIa is the only one that has a long C-terminal, cytoplasmic tail ~50 amino acid residues) (Wu *et al.*, 2009; Desalle *et al.*, 2014), which is known to play a signaling role in, for example, urinary tract infection (Thumbikat *et al.*, 2009). We have confirmed the earlier data by Fukami, Sato, and coworkers that *Xenopus* egg fertilization triggers the phosphorylation of Tyr^{249} located in the cytoplasmic tail of xUPIIIa (Figure 4) (Sakakibara *et al.*, 2005) and showed for the first time that this fertilization-dependent Tyr-phosphorylation of UPIIIa (Tyr^{266}) also occurs in mouse eggs (Figure 5). These results suggest that Tyr phosphorylation of UPIIIa must play a conserved role in egg fertilization. The importance of UPIIIa as a signaling molecule is supported by our recent finding that this protein is evolved from a protein tyrosine phosphatase receptor, a family of cell-surface receptors that initiate intracellular Try-phosphorylation-dependent signal transduction in response to the binding of extracellular ligands (Chicote *et al.*, 2017; Yao *et al.*, 2017).

Fyn is responsible for the tyrosine phosphorylation of UPIIIa. Our data suggesting that Fyn is responsible for Tyr-phosphorylating UPIIIa in mouse egg include the following: 1) uroplakins and Fyn, the major murine egg Src-family kinase (Luo *et al.*, 2009; McGinnis *et al.*, 2011), colocalize forming discrete patches scattered on the surface of mouse eggs both before (Figure 5P) and after fertilization (Figure 5Q), suggesting the formation of a uroplakin/Fyn functional complex; 2) mouse egg fertilization triggers the tyrosine phosphorylation of both Fyn (Tyr^{418}) and UPIIIa (Tyr^{266}; Figure 5, E, K, and Q); and 3) both phosphorylation events are abolished by Src family inhibitor SU6656 (Figure 5, F and L). Complementary data from Fukami, Sato, and coworkers showed that similar events occur in *Xenopus* eggs: 1) egg fertilization triggers the tyrosine phosphorylation of xSrc (Tyr^{416}) and xUPIIIa (Tyr^{249}) (Sakakibara *et al.*, 2005) (Figure 4, P, Q, V, and W), and 2) when xUPIIIa (without xUPIb) was cotransfected with xSrc into HEK293 cells, they coimmunoprecipitated and xUPIIIa became weakly Tyr phosphorylated (Sakakibara *et al.*, 2005). The mouse and frog data are therefore consistent with each other and, together, suggest that the closely related Fyn and Src are responsible for Tyr-phosphorylating UPIIIa of mouse and frog eggs, respectively (Figures 4 and 5) (Mahbub Hasan *et al.*, 2005; Sakakibara *et al.*, 2005; Sato, 2008).

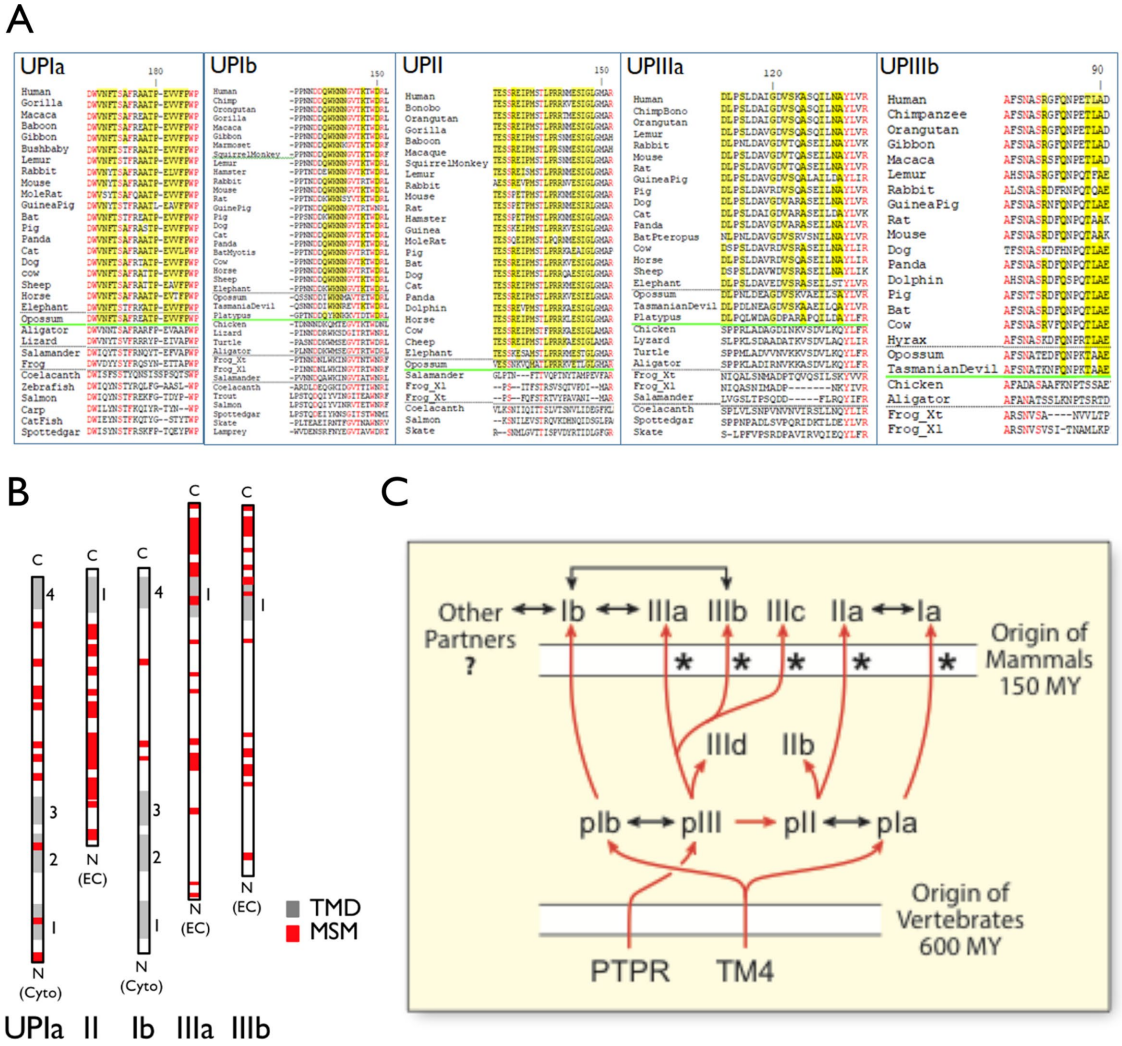

FIGURE 8: Mammal-specific amino acid residues and motifs in uroplakins. (A) Examples of mammal-specific residues (yellow) and amino acid residues that are shared by ALL uroplakins ("all-uroplakin-residues or AUR; red) from UPIa, Ib, II, IIIa, and IIIb of ~20 mammals (17 placental and three nonplacental) and 10 nonmammals (Desalle *et al.*, 2014). Mammal-specific residues are defined as those that are present in >90% of mammals and <30% of nonmammals. The horizontal green line demarcates the sequences of the mammals (above) and nonmammal vertebrates. (B) The overall location of mammal-specific motifs (MSM; red box; greater than three consecutive residues, five with a single interruption, or six with two interruptions) in uroplakins as indicated. TMD (transmembrane domain). (C) Model depicting the evolution of all the known uroplakin genes. Symbols: red arrows (genealogical relationship), two-headed black arrows (protein–protein interaction), asterisk (a strong pattern of significant skew towards *dN*/*dS*>1.0 suggesting possible selection that accompanies the duplication events that produced the paralogue group) (Desalle *et al.*, 2014), phosphotyrosine phosphatase receptor (PTPR) (Chicote *et al.*, 2017), tetraspanin precursor (TM4), million years (MY). See main text for details.

Uroplakin/CD9 interactions. Our results indicate that on mouse egg surface, uroplakins colocalized closely with CD9, forming discrete patches (Figures 3A and 5P), and partially with CD81 (Figure 3B). These results are interesting because both tetraspanins CD9 and CD81 are known to play important roles in mouse egg fertilization (Le Naour *et al.*, 2000; Miyado *et al.*, 2000; Rubinstein *et al.*, 2006) and because uroplakins Ia and Ib are also tetraspanins, which have the propensity to form the "tetraspanin-enriched microdomains" (TEMs) that can enhance signal transduction (Termini and Gillette, 2017). The poor colocalization between uroplakin and the raft marker GM1 (Figure 5R) indicates that the uroplakin-containing TEMs are distinct from the "rafts" (Hemler, 2003; Espenel *et al.*, 2008). The fact that uroplakin/CD9 also colocalize with Fyn (Figure 5, P and Q) further suggests that CD9 may modulate/enhance UPIIIa/Fyn signaling. This idea may seem at odds with an earlier suggestion that xCD9 does not interact with xUPIIIa based on the absence of the former in the uroplakin-containing Triton X-100 resistant raft fraction (Mahbub Hasan *et al.*, 2007). However, this discrepancy can be explained by the fact that tetraspanin association usually does not survive Triton X-100 (Indig *et al.*, 1997; Miao *et al.*, 2001). Indeed, their data showed that centrifugation in Brij 98, but not in Triton, allowed the cofloating of xCD9 with xUPIIIa and xUPIb (Figure 1E in Mahbub Hasan *et al.* [2007]). Finally, even though our data indicate CD9/uroplakin association in mouse egg TEMs (Figure 3A), it remains to be established whether they interact directly (Kovalenko *et al.*, 2004;

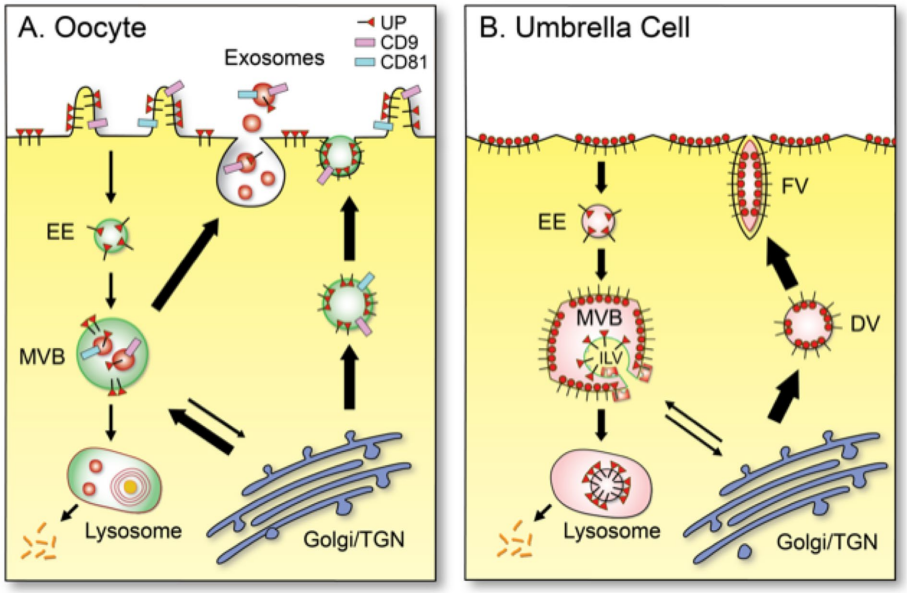

FIGURE 9: Schematic diagrams showing the distinct patterns of uroplakin trafficking in (A) mouse oocyte/egg and (B) a terminally differentiated umbrella cells of mammalian bladder urothelium. (A) In mouse egg, uroplakins (red triangle luminal domain with a cytoplasmic tail; existing possibly as heterotetramers; see *Discussion*) are delivered to the cell surface via exocytosis or to exosomes via MVBs. (B) In urothelial umbrella cells, uroplakins are assembled in *trans*-Golgi network into 16-nm particles (red circles; 16-nm particles), which form growing two-dimensional crystals delivered via DV and FV to the urothelial apical surface, where they form the characteristic urothelial plaques (Wankel *et al.*, 2016). Some of the apical surface-associated uroplakins can be endocytosed into multivesicular vesicles for lysosomal degradation (Vieira *et al.*, 2014). Other abbreviations: EE (early endosome) and TGN (*trans*-Golgi network). Thickness of the arrows approximates the relative abundance of the pathways in the two cell types.

Dahmane *et al.*, 2014) or form separate nanoclusters coexisting in TEMs (Zuidscherwoude *et al.*, 2015).

Remarkable consistency of the mouse and frog data. The remarkable overall consistency between the mouse and *Xenopus* data suggests that uroplakins play a highly conserved role in egg fertilization and that *Xenopus* egg provides a relevant model for studying the biochemical and certain other aspects of uroplakin involvement in this process. In this regard, it should be noted that Sato, Fukami, and coworkers proposed a model, based on their *Xenopus* studies, suggesting that the cleavage of the extracellular domain of xUPIIIa at the juxta-membrane Gly-Arg-Arg (GRR) site by a sperm-derived protease(s) releases the xUPIb/IIIa-inhibition of Src, which then Tyr phosphorylates some of the remaining intact UPIIIa (Mahbub Hasan *et al.*, 2005, 2007, 2014; Hasan *et al.*, 2011). Additional studies are needed to identify the sperm protease(s) hypothesized to be involved in cleaving the juxta-membrane GRR site of the extracellular domain of xUPIIIa, and the functional consequences of UPIIIa phosphorylation, which may include the modulation of its interaction with a downstream target(s) and/or of the physical properties of the egg and/or exosome membranes (see below).

Modulation of membrane stability

Uroplakins enhance membrane rigidity and/or stability. Several lines of evidence suggest that uroplakins enhance the stability and rigidity of the membrane as indicated by enhanced detergent insolubility. As mentioned earlier, uroplakins form two-dimensional crystals of 16-nm particles, the urothelial plaques, which form rigid-looking concave plaques covering the mammalian urothelial apical surface (Hicks, 1965; Kachar *et al.*, 1999). Unlike other tetraspanin-enriched microdomains that can survive only relatively weak detergents such as Brij 99 and CHAPS (Claas *et al.*, 2001), urothelial plaques can largely survive more stringent detergents such as Triton X-100 or Sarkosyl (Wu *et al.*, 1990; Liang *et al.*, 1999). Interestingly, even the regular-looking plasma membranes that interconnect the plaques (the "hinge" areas), which contain no or largely collapsed uroplakin particles, are also insoluble in Triton and Sarkosyl (Liang *et al.*, 1999). This suggests that uroplakins, even when they do not form 16-nm particles, can still enhance urothelial membrane stability as gauged by detergent insolubility. Taken together, these results suggest that uroplakins can increase the stability of membranes in urothelial hinges and possibly the uroplakin/CD9/CD81-containing egg TEM microdomains (Figure 3, A and B). Whether uroplakin mutations can cause fertilization problems in humans is unknown, although it should be noted that sequencing of human CD9 gene, which is critical for egg fertilization in mice, has not revealed any CD9 mutations causing human female fertility problems (Nishiyama *et al.*, 2010), probably because defects in molecules critically important for fertility are subject to negative selection.

Possible structural roles of uroplakins in sperms. Unlike most mammalian sperms that have an oval or paddlelike head, sperms of the myomorph rodents have an apical rostral hook, which contains part of the acrosome. The evolutionary and functional significance of such a unique hook structure is unclear, although it has been suggested to play a role in sperm velocity and postcopulatory competition (Moore *et al.*, 2002; Varea-Sanchez *et al.*, 2016). Since the uroplakin-enriched domain covers the concave (inside) surface of the hook (corresponding possibly to the "hook rim" structure) (Lin *et al.*, 2013), which is far from the acrosome-abutting convex (outside) surface involved in egg binding (Avella and Dean, 2011), this uroplakin-enriched subdomain is unlikely to play a role in sperm–egg interaction. Given the possible roles of uroplakin proteins in enhancing membrane rigidity as discussed above, their association with the inside curvature of the hook including the tip (Figure 6, H–K) suggests a structural role, perhaps in conjunction with the microtubule manchette, in generating and/or maintaining the hook structure. Although UP knockout of males did not affect the sperm morphology (Figure 6, D, E, L, and M) or their ability to fertilize the eggs in our IVF assays and in vivo (Figure 7, C and E), the overwhelmingly high sperm–egg ratio in both of these assays could have masked the suboptimal performance of the UP-deficient sperms.

Evolution of the uroplakin gene family: a unifying model

Our results indicate that uroplakins function in oocytes where they play essential and more ancestral roles in fertilization without forming two-dimensional crystals (Figure 7). Coupled with the fact that mammalian uroplakins have abundant mammal-specific sequences (Figure 8, A and B, and Supplemental Figure S6), these data suggest that uroplakins play highly conserved roles such as egg

fertilization in nonurothelial cells, and that they acquired an additional role in mammalian urothelium. This idea can explain why uroplakin genes have been preserved in most vertebrates, including nonmammals that do not even have a urinary bladder (Garcia-Espana *et al.*, 2006, 2008; Desalle *et al.*, 2014; Chicote *et al.*, 2017), and it can also explain the expression of uroplakins in nonurothelial cells in which uroplakins may perform additional cell type-specific functions.

Although our phylogenetic studies of uroplakin genes shed light on how uroplakin genes are evolved (Garcia-Espana *et al.*, 2006, 2008; Desalle *et al.*, 2014), there are several features of this process remain paradoxical. Here we propose a unifying model of uroplakin gene evolution (Figure 8C), which integrates all our phylogenetic data, including our current findings (Figure 8, A and B, and Supplemental Figure S6), and provides possible explanations for these puzzling features. 1) At the beginning of vertebrates, a tetraspanin-originated proto-UPI gene gave rise to proto-UPIb and proto-UPIa (Garcia-Espana *et al.*, 2006, 2008; Desalle *et al.*, 2014). 2) The proto-UPIb recruited a precursor of the phosphotyrosine phosphatase receptor (PTPR) gene that evolved to become proto-UPIII, which then gave rise to proto-UPII by gene duplication (Chicote *et al.*, 2017); this idea can explain why the UPII sequences are much more distant, than UPIII, from PTPR. 3) The proto-UPII gene gave rise to the current UPIIa (referred to so far as UPII; present in all vertebrates, including mammals) and an early branch of UPIIb that exists only in fish and reptiles; and proto-UPIII gave rise to UPIIIa, UPIIIb, and UPIIIc (present in all vertebrates, including mammals), as well as UPIIId (fish only; corresponds to the UP3a-like protein described in Mitra *et al.* (2012) and Desalle *et al.* (2014). 4) Throughout uroplakin evolution, members within the UPIa/II and UPIb/III pairs strongly coevolved (Garcia-Espana *et al.*, 2006, 2008; Desalle *et al.*, 2014), consistent with their known specific protein/protein interactions (Wu *et al.*, 1995; Tu *et al.*, 2002; Hu *et al.*, 2005). 5) Coinciding with the divergence of mammals, most of the mammalian uroplakins acquired a significant amount of mammal-specific changes (Figure 8, A and B, and Supplemental Figure S6, A–E; asterisks in Figure 8C). Thus, we have identified the evolutionary branches of uroplakins that have experienced statistically significant departure from neutrality in their dN/dS ratios in the uroplakin genealogies, with the single exception of the UPIb (Figure 8C) (Desalle *et al.*, 2014). It is likely that such an acquisition of mammalian-specific sequences forms the basis for neofunctionalization, including two-dimensional crystal formation. 6) There are some data indicating that UPIb protein has a broader tissue distribution than UPIa (Human-Protein-Atlas, [2018]; also see the mRNA data from Lobban *et al.* [1998] and Olsburgh *et al.* [2003]), suggesting that UPIb may interact with additional nonuroplakin partners which may impose extra constraints to UPIb evolution. This can explain why UPIb has undergone the least amount of mammal-specific sequence changes (Figure 8, B and C, and Supplemental Figure S6, A–E) (Desalle *et al.*, 2014). Overall, uroplakin evolution provides a good example of genetic piracy. The ancestral and essential function of uroplakins in, for example, egg fertilization may have locked these genes into the genome. These genes are then pirated during mammal divergence for an additional cellular function, that is, uroepithelial structure, via gene duplication and neofunctionalization.

In conclusion, our data blurred the artificial boundary between the "general" and "specialized" tetraspanins, as uroplakins and their associated proteins, which were thought to be urothelium-specific, are also expressed in several nonurothelial cells, including oocytes of mouse and *Xenopus laevis*, in which they may interact with CD tetraspanins to play conserved and essential roles in fertilization. Only later during mammalian divergence uroplakins acquired ability to form two-dimensional crystalline urothelial plaques to support umbrella cell enlargement, as well as the formation of effective permeability and mechanical barriers (Hu *et al.*, 2000, 2002; Kong *et al.*, 2004), features that are essential for the formation of a functional modern-day mammalian urothelium. Collectively, our data indicate that uroplakins have a broader tissue distribution and play more diverse functions than hitherto appreciated. Additional work is needed to further decipher the functions and disease implications of uroplakins in not just urothelial cells but also nonurothelial cells.

MATERIALS AND METHODS

Reagents and antibodies

The reagents and their sources (in parentheses) are listed below. Hormones gonadotropin from pregnant mare serum (PMSG), chorionic gonadotropin human (hCG); hyaluronidase, acidic Tyrode's solution, reduced L-glutathione (GSH), Src kinase inhibitor SU6656 and Ficoll 400 (Sigma, St. Louis, MO); HEPES-buffered modified human tubal fluid (HTF; Irvine Scientific, Irvine, CA); Research Vitro Fertilization (RVF) medium (Cook Medical, Bloomington, IN); M2 and KSOM media (EMD Millipore Corp., Billerica MA); Ca/Mg-free Quinn's Advantage medium with HEPES (Cooper Surgical, Trumbull, CT); Src kinase inhibitor SKI606 (Selleck Chemicals, Houston, TX); RNeasy Mini Kit (Qiagen, Valencia, CA); Capacity Reverse Transcription Kit (Thermo Fisher Scientific, Waltham, MA); Lowicryl K4M (Polysciences, Warrington, PA); glutaraldehyde, paraformaldehyde, sodium cacodylate, osmium tetroxide, and EMbed 812 (Electron Microscopy Sciences, Hatfield, PA); and HQ Silver enhancement kit (Nanoprobes). See Table 1 for the properties of 10 newly developed mouse monoclonal antibodies to uroplakins (plus the previously described AU1 antibody to UPIIIa) (Liang *et al.*, 2001). See Supplemental Table S1 for a complete list of our anti-uroplakin antibodies, including rabbit polyclonal antibodies against mouse and *Xenopus* uroplakin peptides and subdomains. All our mouse antibodies were purified using Protein G–coupled Sepharose beads, and rabbit antibodies were immunoaffinity-purified using gel-purified uroplakins or synthetic peptides. See Supplemental Table S2 for a list of other antibodies.

Animal strains

The generation and characterization of the UPII-knockout, UPIIIa-knockout, and UPII/UPIIIa double-knockout mice were described earlier (Hu *et al.*, 2000; Kong *et al.*, 2004; Zocher *et al.*, 2012). Oocytes, eggs, and sperms were collected from CB6F1 mice, 6–8 wk of age, from Charles River Laboratories, Wilmington, MA. Mouse tissues were collected from Swiss Webster mice (Taconic Biosciences, Hudson, NY). The *Xenopus* ovaries, eggs, and testis were purchased from Xenopus1.com, Dexter, MI. Our animal work was performed with the approval from the NYU School of Medicine's Institutional Animal Care and Use Committee.

Immunofluorescence staining

Deparaffinized tissue sections were incubated with 5% bovine serum albumin (BSA) in phosphate-buffered saline (PBS) buffer and incubated with primary antibodies at 4°C overnight and later with secondary antibodies for 1 h at room temperature. ZP-free oocytes and eggs were fixed and treated with 0.1% Triton X-100 for 10 min at room temperature, blocked with 5% BSA in PBS buffer, incubated with primary antibodies at 4°C overnight, followed by incubation with secondary antibodies. ZP-intact eggs were incubated with

primary antibodies for 30 min followed by 30 min of fixation at room temperature and then incubated with secondary antibodies for 1 h at room temperature. The oocyte and egg nuclei were costained with either 4′,6-diamidino-2-phenylindole (DAPI; permeabilized) or Hoechst 33258 (nonpermeabilized). Mouse sperms were collected from caput and cauda epididymis as described in the IVF method, fixed with 4% formaldehyde and permeabilized with 0.1% Triton X-100, blocked with 5% BSA, and incubated with primary antibodies and costained with DAPI.

Electron microscopy

Mouse ovaries and eggs were fixed in the fixative containing 2.5% glutaraldehyde and 2% paraformaldehyde in 0.1 M sodium cacodylate buffer (pH 7.2) for 2 h, postfixed with 1% osmium tetroxide for 1.5 h at room temperature, and then processed in a standard manner and embedded in EMbed 812 for transmission electron microscopy. For immunoelectron microscopy, mouse eggs were fixed in freshly made 3% paraformaldehyde in 0.1 M sodium cacodylate buffer containing 0.1% glutaraldehyde and 4% sucrose (pH 7.4). After washing and dehydration, the tissues were embedded in Lowicryl K4M and polymerized under UV (360 nm) at 35°C. Ultrathin sections were mounted on formvar-/carbon-coated nickel grids, incubated with primary antibodies at 4°C overnight and then with nanogold- or 18-nm colloidal gold-conjugated secondary antibodies followed by silver enhancement in the dark for 8 min. Grids were stained with uranyl acetate and lead citrate by standard methods, examined with a Philips CM12 electron microscope (FEI, Eindhoven, The Netherlands) and photographed with a Gatan (4 k × 2.7 k) digital camera (Gatan, Pleasanton, CA).

RT-PCR

Total RNA was prepared using the RNeasy Mini Kit; RNA concentration was determined using Nanodrop (Thermo Scientific, Waltham, MA); RT-PCR was performed on a GeneAmp PCR System (Applied Biosystems, Foster City, CA); and PCR products were analyzed by electrophoresis on 2% agarose gels stained with ethidium bromide.

Hormonal priming, antibody blocking, and in vitro fertilization

Female wild-type (WT), UPII KO, UPIIIa KO, and UPII- and UPIIIa double-KO mice were injected intraperitoneally with 10 IU of PMSG for 48 h and then 10 IU of hCG for 15 h before killing. IVF and in vitro culture IVF procedures were modified from (Hogan, 1994; Chang *et al.*, 2005). Male mice were killed by cervical dislocation under anesthesia. The vas deferens was cut close to the cauda epididymis, and the sperms were extruded into a dish containing HEPES-HTF medium. The dish was then placed in a 37°C incubator for 0.5 h for sperm swimming out and capacitation. Freshly mature eggs were placed into dishes containing 250-µl drops of high calcium (5.14 mM) RVF medium with 1 mM GSH covered by mineral oil. Sperm mixture (5–10 µl) was pipetted to each microdrop to a final concentration of (1–2) × 10^6 sperm/ml. After 56 h of coincubation at 37°C, the two-cell stage embryos were collected and washed with M2 medium and then transferred to microdrop of KSOM and placed in a 5% CO_2 incubator at 37°C. The embryos were monitored daily and cultured to blastocyst stage. The mature eggs were collected from female CB6F1 mice injected with PMSG and HCG and treated with hyaluronidase (300 IU/ml) in HEPES-HTF medium to remove cumulus cells. After three washes, mature eggs were transferred into five drops of RVF medium, which contained the antibodies against UPIa, UPIb, UPIIIa, CD9, and normal rabbit immunoglobulin G (IgG) (200 µg/ml each), respectively, and incubated in the 5% CO_2 for 30 min at 37°C. The eggs then were washed three times in fresh drops of media, and regular IVF was performed as described above.

Collection of mouse tissues, oocytes, and eggs

Urinary bladder, eye, kidney, prostate, epididymis, stomach, ovary, testis, and oviduct with ovulated eggs were collected from Swiss Webster, CB6F1, UPII KO, and UPIIIa KO mice, fixed in 4% formaldehyde and embedded in paraffin, and sectioned (4 µm thick). Immature oocytes (Prophase I arrested) were obtained from the ovaries of female CB6F1 mice in HTF-BSA medium (modified from Kryzak *et al.* [2013]). The mature egg collection procedure was modified from those of Hogan (1994). The cumulus egg complexes were obtained from the oviduct of CB6F1 mice. Then cumulus cells were removed mechanically by pipetting vigorously in HEPES-HTF medium + hyaluronidase (300 IU/ml). The oocytes and eggs were transferred to acidic Tyrode's solution, pH 2.5, for 1–2 min to remove the zona pellucida. The eggs were washed three times with HEPES-HTF medium and then fixed with 4% formaldehyde for 1 h at room temperature.

Parthenogenetic activation and inhibitor treatment of mouse and *Xenopus* eggs

The mouse experiments were done according to Cuthbertson (1983) with modification. Briefly, mouse eggs were treated to remove the zona pellucida and split into two groups. One group was kept in Quinn's medium with 1% BSA (Quinn's BSA), plus 5 µM SU6656, and the other group was kept in Quinn's BSA plus dimethyl sulfoxide (DMSO). After incubation for 30 min at 37°C, half of the eggs from each group were transferred to fresh Quinn's medium at 37°C, and the other half was exposed to 8% ethanol in Quinn's medium at 37°C, 5% CO_2 for 6.5 min. The eggs were washed three times with Quinn's medium and then fixed with 4% formaldehyde. The *Xenopus* fertilization experiments were done according to Sakakibara *et al.* (2005) with minor modifications. The eggs were divided into three groups. In Group A, the eggs were incubated with normal rabbit IgG (100 µg/ml) or affinity-purified xIIIa IgG in fertilization buffer plus 1% BSA for 30 min at room temperature, then washed with fertilization buffer three times. The eggs were then incubated with sperms for 10 min. In Group B, eggs were incubated with 500 mM H_2O_2 in fertilization buffer for 2 min at room temperature. In Group C, eggs were incubated with 2-µM SKI606 in fertilization buffer for 30 min at room temperature. Finally, some eggs were kept in fertilization buffer with DMSO as controls. After three washes, the eggs of Groups A and C were also treated with H_2O_2. All three groups of eggs were washed with fertilization buffer three times after the treatments and fixed with 4% formaldehyde.

ACKNOWLEDGMENTS

We thank Michael J. Rindler and Ping Zhou for their advice and help in this project and Jurrien Dean of the National Institutes of Health (NIH)/National Institute of Diabetes and Digestive and Kidney Diseases for the ovastacin antiserum. We acknowledge the excellent services by our institute's Core Laboratories on Microscopy, Experimental Pathology, and Rodent Genetic Engineering, which are supported in part by NIH grants NCRR RR023704 and RR024708. This work was supported by grants from the NIH, DK52206 (T.-T.S. and X.R.W.) and DK39753 and DK110466 (T.-T.S.); and Spanish Ministerio de Economía y Competitividad FIS PI16/00504 (A.G.-E.).

REFERENCES

Adachi W, Okubo K, Kinoshita S (2000). Human uroplakin Ib in ocular surface epithelium. Invest Ophthalmol Vis Sci 41, 2900–2905.

Ahmad I, Singh LB, Foth M, Morris CA, Taketo MM, Wu XR, Leung HY, Sansom OJ, Iwata T (2011). K-Ras and beta-catenin mutations cooperate with Fgfr3 mutations in mice to promote tumorigenesis in the skin and lung, but not in the bladder. Dis Model Mech 4, 548–555.

Avella MA, Dean J (2011). Fertilization with acrosome-reacted mouse sperm: implications for the site of exocytosis. Proc Natl Acad Sci USA 108, 19843–19844.

Ayala de la Pena F, Kanasaki K, Kanasaki M, Vong S, Rovira C, Kalluri R (2014). Specific activation of K-RasG12D allele in the bladder urothelium results in lung alveolar and vascular defects. PLoS One 9, e95888.

Berditchevski F, Rubinstein E (2013). Tetraspanins, Vol 9 (Springer).

Carpenter AR, Becknell MB, Ching CB, Cuaresma EJ, Chen X, Hains DS, McHugh KM (2016). Uroplakin 1b is critical in urinary tract development and urothelial differentiation and homeostasis. Kidney Int 89, 612–624.

Chang HC, Liu H, Zhang J, Grifo J, Krey LC (2005). Developmental incompetency of denuded mouse oocytes undergoing maturation in vitro is ooplasmic in nature and is associated with aberrant Oct-4 expression. Hum Reprod 20, 1958–1968.

Charrin S, Jouannet S, Boucheix C, Rubinstein E (2014). Tetraspanins at a glance. J Cell Sci 127, 3641–3648.

Chicote JU, DeSalle R, Segarra J, Sun T-T, Garcia-Espana A (2017). The tetraspanin-associated uroplakins family (UPK2/3) is evolutionarily related to PTPRQ, a phosphotyrosine phosphatase receptor. PLoS One 12, e0170196.

Claas C, Stipp CS, Hemler ME (2001). Evaluation of prototype transmembrane 4 superfamily protein complexes and their relation to lipid rafts. J Biol Chem 276, 7974–7984.

Cuthbertson KS (1983). Parthenogenetic activation of mouse oocytes in vitro with ethanol and benzyl alcohol. J Exp Zool 226, 311–314.

Dahmane S, Rubinstein E, Milhiet PE (2014). Viruses and tetraspanins: lessons from single molecule approaches. Viruses 6, 1992–2011.

Deng FM, Liang FX, Tu L, Resing KA, Hu P, Supino M, Hu CC, Zhou G, Ding M, Kreibich G, *et al*. (2002). Uroplakin IIIb, a urothelial differentiation marker, dimerizes with uroplakin Ib as an early step of urothelial plaque assembly. J Cell Biol 159, 685–694.

Desalle R, Chicote JU, Sun T-T, Garcia-Espana A (2014). Generation of divergent uroplakin tetraspanins and their partners during vertebrate evolution: identification of novel uroplakins. BMC Evol Biol 14, 13.

Espenel C, Margeat E, Dosset P, Arduise C, Le Grimellec C, Royer CA, Boucheix C, Rubinstein E, Milhiet PE (2008). Single-molecule analysis of CD9 dynamics and partitioning reveals multiple modes of interaction in the tetraspanin web. J Cell Biol 182, 765–776.

Evans JP (2012). Sperm-egg interaction. Annu Rev Physiol 74, 477–502.

Gallo LI, Dalghi MG, Clayton DR, Ruiz WG, Khandelwal P, Apodaca G (2018). RAB27B requirement for stretch-induced exocytosis in bladder umbrella cells. Am J Physiol Cell Physiol 314, C349–C365.

Garcia-Espana A, Chung PJ, Sarkar IN, Stiner E, Sun T-T, Desalle R (2008). Appearance of new tetraspanin genes during vertebrate evolution. Genomics 91, 326–334.

Garcia-Espana A, Chung PJ, Zhao X, Lee A, Pellicer A, Yu J, Sun T-T, Desalle R (2006). Origin of the tetraspanin uroplakins and their co-evolution with associated proteins: implications for uroplakin structure and function. Mol Phylogenet Evol 41, 355–367.

Goldberg AF, Moritz OL, Williams DS (2016). Molecular basis for photoreceptor outer segment architecture. Prog Retin Eye Res 55, 52–81.

Guha A, Deshpande A, Jain A, Sebastiani P, Cardoso WV (2017). *Uroplakin 3a(+) cells are a distinctive population of epithelial progenitors that contribute to airway maintenance and post-injury repair. Cell Rep 19, 246–254.

Harada Y, Yoshida K, Kawano N, Miyado K (2013). Critical role of exosomes in sperm-egg fusion and virus-induced cell-cell fusion. Reprod Med Biol 12, 117–126.

Hasan AK, Fukami Y, Sato K (2011). Gamete membrane microdomains and their associated molecules in fertilization signaling. Mol Reprod Dev 78, 814–830.

Hemler ME (2003). Tetraspanin proteins mediate cellular penetration, invasion, and fusion events and define a novel type of membrane microdomain. Annu Rev Cell Dev Biol 19, 397–422.

Hemler ME (2005). Tetraspanin functions and associated microdomains. Nat Rev Mol Cell Biol 6, 801–811.

Hicks RM (1965). The fine structure of the transitional epithelium of rat ureter. J Cell Biol 26, 25–48.

Hoang LL, Tacha D, Bremer RE, Haas TS, Cheng L (2015). Uroplakin II (UPII), GATA3, and p40 are highly sensitive markers for the differential diagnosis of invasive urothelial carcinoma. Appl Immunohistochem Mol Morphol 23, 711–716.

Hogan B (1994). Manipulating the Mouse Embryo: A Laboratory Manual, Cold Spring Harbor, NY: Cold Spring Harbor Laboratory Press.

Hu CC, Bachmann T, Zhou G, Liang FX, Ghiso J, Kreibich G, Sun T-T (2008). Assembly of a membrane receptor complex: roles of the uroplakin II prosequence in regulating uroplakin bacterial receptor oligomerization. Biochem J 414, 195–203.

Hu CC, Liang FX, Zhou G, Tu L, Tang CH, Zhou J, Kreibich G, Sun T-T (2005). Assembly of urothelial plaques: tetraspanin function in membrane protein trafficking. Mol Biol Cell 16, 3937–3950.

Hu P, Deng FM, Liang FX, Hu CM, Auerbach AB, Shapiro E, Wu XR, Kachar B, Sun T-T (2000). Ablation of uroplakin III gene results in small urothelial plaques, urothelial leakage, and vesicoureteral reflux. J Cell Biol 151, 961–972.

Hu P, Meyers S, Liang FX, Deng FM, Kachar B, Zeidel ML, Sun T-T (2002). Role of membrane proteins in permeability barrier function: uroplakin ablation elevates urothelial permeability. Am J Physiol Renal Physiol 283, F1200–F1207.

Huang HY, Shariat SF, Sun T-T, Lepor H, Shapiro E, Hsieh JT, Ashfaq R, Lotan Y, Wu XR (2007). Persistent uroplakin expression in advanced urothelial carcinomas: implications in urothelial tumor progression and clinical outcome. Hum Pathol 38, 1703–1713.

Human-Protein-Atlas (2018) www.proteinatlas.org (accessed September 2018).

Indig FE, Diaz-Gonzalez F, Ginsberg MH (1997). Analysis of the tetraspanin CD9-integrin alphaIIbbeta3 (GPIIb-IIIa) complex in platelet membranes and transfected cells. Biochem J 327 (Pt 1), 291–298.

Jenkins D, Bitner-Glindzicz M, Malcolm S, Hu CC, Allison J, Winyard PJ, Gullett AM, Thomas DF, Belk RA, Feather SA, *et al*. (2005). De novo Uroplakin IIIa heterozygous mutations cause human renal adysplasia leading to severe kidney failure. J Am Soc Nephrol 16, 2141–2149.

Kachar B, Liang F, Lins U, Ding M, Wu XR, Stoffler D, Aebi U, Sun T-T (1999). Three-dimensional analysis of the 16 nm urothelial plaque particle: luminal surface exposure, preferential head-to-head interaction, and hinge formation. J Mol Biol 285, 595–608.

Kanamori-Katayama M, Kaiho A, Ishizu Y, Okamura-Oho Y, Hino O, Abe M, Kishimoto T, Sekihara H, Nakamura Y, Suzuki H, *et al*. (2011). LRRN4 and UPK3B are markers of primary mesothelial cells. PLoS One 6, e25391.

Khandelwal P, Abraham SN, Apodaca G (2009). Cell biology and physiology of the uroepithelium. Am J Physiol Renal Physiol 297, F1477–F1501.

Kong XT, Deng FM, Hu P, Liang FX, Zhou G, Auerbach AB, Genieser N, Nelson PK, Robbins ES, Shapiro E, *et al*. (2004). Roles of uroplakins in plaque formation, umbrella cell enlargement, and urinary tract diseases. J Cell Biol 167, 1195–1204.

Kovalenko OV, Yang X, Kolesnikova TV, Hemler ME (2004). Evidence for specific tetraspanin homodimers: inhibition of palmitoylation makes cysteine residues available for cross-linking. Biochem J 377, 407–417.

Kryzak CA, Moraine MM, Kyle DD, Lee HJ, Cubenas-Potts C, Robinson DN, Evans JP (2013). Prophase I mouse oocytes are deficient in the ability to respond to fertilization by decreasing membrane receptivity to sperm and establishing a membrane block to polyspermy. Biol Reprod 89, 44.

Le Naour F, Andre M, Boucheix C, Rubinstein E (2006). Membrane microdomains and proteomics: lessons from tetraspanin microdomains and comparison with lipid rafts. Proteomics 6, 6447–6454.

Le Naour F, Rubinstein E, Jasmin C, Prenant M, Boucheix C (2000). Severely reduced female fertility in CD9-deficient mice. Science 287, 319–321.

Liang F, Kachar B, Ding M, Zhai Z, Wu XR, Sun T-T (1999). Urothelial hinge as a highly specialized membrane: detergent- insolubility, urohingin association, and in vitro formation. Differentiation 65, 59–69.

Liang FX, Bosland MC, Huang H, Romih R, Baptiste S, Deng FM, Wu XR, Shapiro E, Sun T-T (2005). Cellular basis of urothelial squamous metaplasia: roles of lineage heterogeneity and cell replacement. J Cell Biol 171, 835–844.

Liang FX, Riedel I, Deng FM, Zhou G, Xu C, Wu XR, Kong XP, Moll R, Sun T-T (2001). Organization of uroplakin subunits: transmembrane topology, pair formation and plaque composition. Biochem J 355, 13–18.

Lin JH, Zhao H, Sun T-T (1995). A tissue-specific promoter that can drive a foreign gene to express in the suprabasal urothelial cells of transgenic mice. Proc Natl Acad Sci USA 92, 679–683.

Lin YW, Hsu TH, Yen PH (2013). Mouse sperm acquire a new structure on the apical hook during epididymal maturation. Asian J Androl 15, 523–528.

Lobban ED, Smith BA, Hall GD, Harnden P, Roberts P, Selby PJ, Trejdosiewicz LK, Southgate J (1998). Uroplakin gene expression by normal and neoplastic human urothelium. Am J Pathol 153, 1957–1967.

Luo J, McGinnis LK, Kinsey WH (2009). Fyn kinase activity is required for normal organization and functional polarity of the mouse oocyte cortex. Mol Reprod Dev 76, 819–831.

Mahbub Hasan AK, Hashimoto A, Maekawa Y, Matsumoto T, Kushima S, Ijiri TW, Fukami Y, Sato K (2014). The egg membrane microdomain-associated uroplakin III-Src system becomes functional during oocyte maturation and is required for bidirectional gamete signaling at fertilization in Xenopus laevis. Development 141, 1705–1714.
Mahbub Hasan AK, Ou Z, Sakakibara K, Hirahara S, Iwasaki T, Sato K, Fukami Y (2007). Characterization of Xenopus egg membrane microdomains containing uroplakin Ib/III complex: roles of their molecular interactions for subcellular localization and signal transduction. Genes Cells 12, 251–267.
Mahbub Hasan AK, Sato K, Sakakibara K, Ou Z, Iwasaki T, Ueda Y, Fukami Y (2005). Uroplakin III, a novel Src substrate in Xenopus egg rafts, is a target for sperm protease essential for fertilization. Dev Biol 286, 483–492.
McGinnis LK, Carroll DJ, Kinsey WH (2011). Protein tyrosine kinase signaling during oocyte maturation and fertilization. Mol Reprod Dev 78, 831–845.
Meldolesi J (2018). Exosomes and ectosomes in intercellular communication. Curr Biol 28, R435–R444.
Miao WM, Vasile E, Lane WS, Lawler J (2001). CD36 associates with CD9 and integrins on human blood platelets. Blood 97, 1689–1696.
Min G, Wang H, Sun T-T, Kong XP (2006). Structural basis for tetraspanin functions as revealed by the cryo-EM structure of uroplakin complexes at 6-A resolution. J Cell Biol 173, 975–983.
Mitra S, Lukianov S, Ruiz WG, Cianciolo Cosentino C, Sanker S, Traub LM, Hukriede NA, Apodaca G (2012). Requirement for a uroplakin 3a-like protein in the development of zebrafish pronephric tubule epithelial cell function, morphogenesis, and polarity. PLoS One 7, e41816.
Miyado K, Yamada G, Yamada S, Hasuwa H, Nakamura Y, Ryu F, Suzuki K, Kosai K, Inoue K, Ogura A, *et al.* (2000). Requirement of CD9 on the egg plasma membrane for fertilization. Science 287, 321–324.
Moll R, Wu XR, Lin JH, Sun T-T (1995). Uroplakins, specific membrane proteins of urothelial umbrella cells, as histological markers of metastatic transitional cell carcinomas. Am J Pathol 147, 1383–1397.
Moore H, Dvorakova K, Jenkins N, Breed W (2002). Exceptional sperm cooperation in the wood mouse. Nature 418, 174–177.
Morita E, Sandrin V, Chung HY, Morham SG, Gygi SP, Rodesch CK, Sundquist WI (2007). Human ESCRT and ALIX proteins interact with proteins of the midbody and function in cytokinesis. EMBO J 26, 4215–4227.
Negrete HO, Lavelle JP, Berg J, Lewis SA, Zeidel ML (1996). Permeability properties of the intact mammalian bladder epithelium. Am J Physiol 271, F886–F894.
Nishiyama S, Kishi T, Kato T, Suzuki M, Nishizawa H, Pryor-Koishi K, Sawada T, Nishiyama Y, Iwata N, Udagawa Y, *et al.* (2010). CD9 gene variations are not associated with female infertility in humans. Gynecol Obstet Invest 69, 116–121.
Olsburgh J, Harnden P, Weeks R, Smith B, Joyce A, Hall G, Poulsom R, Selby P, Southgate J (2003). Uroplakin gene expression in normal human tissues and locally advanced bladder cancer. J Pathol 199, 41–49.
Pisitkun T, Shen RF, Knepper MA (2004). Identification and proteomic profiling of exosomes in human urine. Proc Natl Acad Sci USA 101, 13368–13373.
Romih R, Veranic P, Jezernik K (2002). Appraisal of differentiation markers in urothelial cells. Appl Immunohistochem Mol Morphol 10, 339–343.
Rubinstein E, Ziyyat A, Prenant M, Wrobel E, Wolf JP, Levy S, Le Naour F, Boucheix C (2006). Reduced fertility of female mice lacking CD81. Dev Biol 290, 351–358.
Rudat C, Grieskamp T, Rohr C, Airik R, Wrede C, Hegermann J, Herrmann BG, Schuster-Gossler K, Kispert A (2014). Upk3b is dispensable for development and integrity of urothelium and mesothelium. PLoS One 9, e112112.
Sakakibara K, Sato K, Yoshino K, Oshiro N, Hirahara S, Mahbub Hasan AK, Iwasaki T, Ueda Y, Iwao Y, Yonezawa K, *et al.* (2005). Molecular identification and characterization of Xenopus egg uroplakin III, an egg raft-associated transmembrane protein that is tyrosine-phosphorylated upon fertilization. J Biol Chem 280, 15029–15037.
Sato K (2008). Signal transduction of fertilization in frog eggs and anti-apoptotic mechanism in human cancer cells: common and specific functions of membrane microdomains. Open Biochem J 2, 49–59.
Schnegelsberg B, Sun TT, Cain G, Bhattacharya A, Nunn PA, Ford AP, Vizzard MA, Cockayne DA (2010). Overexpression of NGF in mouse urothelium leads to neuronal hyperinnervation, pelvic sensitivity, and changes in urinary bladder function. Am J Physiol Regul Integr Comp Physiol 298, R534–R547.
Stuck MW, Conley SM, Naash MI (2016). PRPH2/RDS and ROM-1: Historical context, current views and future considerations. Prog Retin Eye Res 52, 47–63.
Sun T-T, Kreibich G, Pellicer A, Kong XP, Wu XR (2013). Uroplakins as a unique tetraspanin network. In: Tetraspanins, ed. F. Berditchevski and E. Rubinstein, Dordrecht, Netherlands: Springer, 299–320.
Swamynathan SK, Davis J, Piatigorsky J (2008). Identification of candidate Klf4 target genes reveals the molecular basis of the diverse regulatory roles of Klf4 in the mouse cornea. Invest Ophthalmol Vis Sci 49, 3360–3370.
Termini CM, Gillette JM (2017). Tetraspanins function as regulators of cellular signaling. Front Cell Dev Biol 5, 34.
Thumbikat P, Berry RE, Zhou G, Billips BK, Yaggie RE, Zaichuk T, Sun T-T, Schaeffer AJ, Klumpp DJ (2009). Bacteria-induced uroplakin signaling mediates bladder response to infection. PLoS Pathog 5, e1000415.
Tian W, Guner G, Miyamoto H, Cimino-Mathews A, Gonzalez-Roibon N, Argani P, Li X, Sharma R, Subhawong AP, Rezaei K, *et al.* (2015). Utility of uroplakin II expression as a marker of urothelial carcinoma. Hum Pathol 46, 58–64.
Tu L, Sun T-T, Kreibich G (2002). Specific heterodimer formation is a prerequisite for uroplakins to exit from the endoplasmic reticulum. Mol Biol Cell 13, 4221–4230.
Van Batavia J, Yamany T, Molotkov A, Dan H, Mansukhani M, Batourina E, Schneider K, Oyon D, Dunlop M, Wu XR, *et al.* (2014). Bladder cancers arise from distinct urothelial sub-populations. Nat Cell Biol 16, 982–991, 981–985.
van Deventer SJ, Dunlock VE, van Spriel AB (2017). Molecular interactions shaping the tetraspanin web. Biochem Soc Trans 45, 741–750.
Varea-Sanchez M, Tourmente M, Bastir M, Roldan ER (2016). Unraveling the sperm bauplan: relationships between sperm head morphology and sperm function in rodents. Biol Reprod 95, 25.
Vieira N, Deng FM, Liang FX, Liao Y, Chang J, Zhou G, Zheng W, Simon JP, Ding M, Wu XR, *et al.* (2014). SNX31: a novel sorting nexin associated with the uroplakin-degrading multivesicular bodies in terminally differentiated urothelial cells. PLoS One 9, e99644.
Wang H, Min G, Glockshuber R, Sun T-T, Kong XP (2009). Uropathogenic E. coli adhesin-induced host cell receptor conformational changes: implications in transmembrane signaling transduction. J Mol Biol 392, 352–361.
Wankel B, Ouyang J, Guo X, Hadjiolova K, Miller J, Liao Y, Tham DK, Romih R, Andrade LR, Gumper I, *et al.* (2016). Sequential and compartmentalized action of Rabs, SNAREs, and MAL in the apical delivery of fusiform vesicles in urothelial umbrella cells. Mol Biol Cell 27, 1621–1634.
Wu XR (2009). Biology of urothelial tumorigenesis: insights from genetically engineered mice. Cancer Metastasis Rev 28, 281–290.
Wu XR, Kong XP, Pellicer A, Kreibich G, Sun T-T (2009). Uroplakins in urothelial biology, function, and disease. Kidney Int 75, 1153–1165.
Wu XR, Lin JH, Walz T, Haner M, Yu J, Aebi U, Sun T-T (1994). Mammalian uroplakins. A group of highly conserved urothelial differentiation-related membrane proteins. J Biol Chem 269, 13716–13724.
Wu XR, Manabe M, Yu J, Sun T-T (1990). Large scale purification and immunolocalization of bovine uroplakins I, II, and III. Molecular markers of urothelial differentiation. J Biol Chem 265, 19170–19179.
Wu XR, Medina JJ, Sun T-T (1995). Selective interactions of UPIa and UPIb, two members of the transmembrane 4 superfamily, with distinct single transmembrane-domained proteins in differentiated urothelial cells. J Biol Chem 270, 29752–29759.
Yao Z, Darowski K, St-Denis N, Wong V, Offensperger F, Villedieu A, Amin S, Malty R, Aoki H, Guo H, *et al.* (2017). A global analysis of the receptor tyrosine kinase-protein phosphatase Interactome. Mol Cell 65, 347–360.
Yu J, Manabe M, Wu XR, Xu C, Surya B, Sun T-T (1990). Uroplakin I: a 27-kD protein associated with the asymmetric unit membrane of mammalian urothelium. J Cell Biol 111, 1207–1216.
Zhou H, Liu Y, He F, Mo L, Sun TT, Wu XR (2010). Temporally and spatially controllable gene expression and knockout in mouse urothelium. Am J Physiol Renal Physiol 299, F387–F395.
Zocher F, Zeidel ML, Missner A, Sun T-T, Zhou G, Liao Y, von Bodungen M, Hill WG, Meyers S, Pohl P, *et al.* (2012). Uroplakins do not restrict CO2 transport through urothelium. J Biol Chem 287, 11011–11017.
Zuidscherwoude M, Gottfert F, Dunlock VM, Figdor CG, van den Bogaart G, van Spriel AB (2015). The tetraspanin web revisited by super-resolution microscopy. Sci Rep 5, 12201.